NAVAL POSTGRADUATE SCHOOL
Monterey, California

THESIS

DESIGN OF MICROSTRIP PATCH ANTENNA FOR THE NPSAT1

by

Mahmut Erel

December 2002

Thesis Advisor:	Jovan E. Lebaric
Second Reader:	Richard W. Adler

Approved for public release; distribution is unlimited.

THIS PAGE INTENTIONALLY LEFT BLANK

REPORT DOCUMENTATION PAGE			Form Approved OMB No. 0704-0188
Public reporting burden for this collection of information is estimated to average 1 hour per response, including the time for reviewing instruction, searching existing data sources, gathering and maintaining the data needed, and completing and reviewing the collection of information. Send comments regarding this burden estimate or any other aspect of this collection of information, including suggestions for reducing this burden, to Washington headquarters Services, Directorate for Information Operations and Reports, 1215 Jefferson Davis Highway, Suite 1204, Arlington, VA 22202-4302, and to the Office of Management and Budget, Paperwork Reduction Project (0704-0188) Washington DC 20503.			
1. AGENCY USE ONLY *(Leave blank)*	**2. REPORT DATE** December 2002	**3. REPORT TYPE AND DATES COVERED** Master's Thesis	
4. TITLE AND SUBTITLE: Design of Microstrip Patch Antenna for the NPSAT1			**5. FUNDING NUMBERS**
6. AUTHOR (S) Mahmut Erel			
7. PERFORMING ORGANIZATION NAME (S) AND ADDRESS (ES) Naval Postgraduate School Monterey, CA 93943-5000			**8. PERFORMING ORGANIZATION REPORT NUMBER**
9. SPONSORING /MONITORING AGENCY NAME (S) AND ADDRESS (ES) N/A			**10. SPONSORING/MONITORING AGENCY REPORT NUMBER**
11. SUPPLEMENTARY NOTES The views expressed in this thesis are those of the author and do not reflect the official policy or position of the Department of Defense or the U.S. Government.			
12a. DISTRIBUTION / AVAILABILITY STATEMENT Approved for public release; distribution is unlimited.			**12b. DISTRIBUTION CODE**
13. ABSTRACT (maximum 200 words) This thesis presents the design of two circularly polarized patch antennas for operation at 1.767 GHz and at 2.207 GHz (for receiving and transmitting, respectively) on NPSAT1 satellite. The design requirements for the antennas include a VSWR of less than or equal to 2:1 for 50 Ω reference impedance. The study includes of the development of a three-dimensional antenna model, antenna simulation, and analysis of results based on various outputs of the CST Microwave Studio Finite Difference Time Domain (FDTD) software package.			
14. SUBJECT TERMS Microstrip Patch Antenna, NPSAT1, Narrow—band, Low Power Satellite Antennas, Elliptical Patch, FDTD Electromagnetic Modeling, Patch Antenna Simulation.			**15. NUMBER OF PAGES** 82
			16. PRICE CODE
17. SECURITY CLASSIFICATION OF REPORT Unclassified	**18. SECURITY CLASSIFICATION OF THIS PAGE** Unclassified	**19. SECURITY CLASSIFICATION OF ABSTRACT** Unclassified	**20. LIMITATION OF ABSTRACT** UL

NSN 7540-01-280-5500

Standard Form 298 (Rev. 2-89)
Prescribed by ANSI Std. 239-18

THIS PAGE INTENTIONALLY LEFT BLANK

Approved for public release; distribution is unlimited.

DESIGN OF A MICROSTRIP PATCH ANTENNA FOR THE NPSAT1

Mahmut Erel
Lieutenant Junior Grade, Turkish Navy
B.S.E.E., Turkish Naval Academy, Istanbul, 1996

Submitted in partial fulfillment of the
requirements for the degree of

MASTER OF SCIENCE IN ELECTRICAL ENGINEERING

from the

NAVAL POSTGRADUATE SCHOOL
December 2002

Author: Mahmut Erel

Approved by: Jovan E. Lebaric
Thesis Advisor

Richard W. Adler
Second Reader

John Powers
Chairman, Department of Electrical and Computer Engineering

THIS PAGE INTENTIONALLY LEFT BLANK

ABSTRACT

This thesis presents the design of two circularly polarized patch antennas for operation at 1.767 GHz and at 2.207 GHz (for receiving and transmitting, respectively) on NPSAT1 satellite. The design requirements for the antennas include a VSWR of less than or equal to 2:1 for 50 Ω reference impedance. The study includes of the development of a three-dimensional antenna model, antenna simulation, and analysis of results based on various outputs of the CST Microwave Studio Finite Difference Time Domain (FDTD) software package.

THIS PAGE INTENTIONALLY LEFT BLANK

TABLE OF CONTENTS

I. INTRODUCTION 1
- A. STATEMENT OF THE PROBLEM 1
  - 1. Background 1
  - 2. Problem 1
- B. SCOPE AND LIMITATIONS 2
  - 1. Scope 2
  - 2. Limitations 2
- C. OBJECTIVES OF THE STUDY 2
- D. BENEFIT OF THE STUDY 3
- E. GENERAL BACKGROUND OF THE NPSAT1 3
  - 1. Mission Objectives 3
  - 2. Spacecraft Description 3

II. CIRCULARLY POLARIZED MICROSTRIP PATCH ANTENNAS 9
- A. DEFINITION OF POLARIZATION 9
- B. CIRCULAR POLARIZATION FOR PATCH ANTENNAS 9

III. DESIGN OF THE ANTENNA AND COMPONENTS 15
- A. DESIGN METHODOLOGY 15
  - 1. Design Techniques and Software 15
  - 2. NPSAT1 Relative Position and Coordinate System Used 19
- B. GENERAL DESCRIPTION OF THE ANTENNA ASSEMBLY 21

IV. ELECTROMAGNETIC SIMULATION RESULTS 31
- A. VSWR AS A FUNCTION OF FREQUENCY 31
  - 1. VSWR for the Receive Antenna 31
  - 2. VSWR for the Transmit Antenna 32
  - 3. Port Signals 34
  - 4. S- Parameters 34
    - *a. S-Parameter Magnitude 35*
    - *b. Mutual Coupling S-Parameter Magnitude 36*
    - *c. S-Parameter Smith Charts 37*
- B. FARFIELD SIMULATION RESULTS 39
  - 1. Radiation Patterns for the Receive Antenna 39
  - 2. Simulation Results for the Transmit Antenna 44

V. CONCLUSIONS AND RECOMMENDATIONS 51
- A. CONCLUSIONS 51
- B. RECOMMENDATIONS 51

APPENDIX A. PHYSICAL DIMENSIONS OF THE RECEIVE ANTENNA 53

APPENDIX B. PHYSICAL DIMENSIONS OF THE TRANSMIT ANTENNA 55

APPENDIX C. ANTENNA VSWR VS. REFLECTION COEFFICIENT 57

LIST OF REFERENCES **59**
BIBLIOGRAPHY **61**
INITIAL DISTRIBUTION LIST **63**

LIST OF FIGURES

Figure 1. NPSAT1 Existing Structure and Solar Panels 5
Figure 2. NPSAT1 Expanded View [From NPSAT1 Design Team.].....6
Figure 3. Basic Radiating Elements for Linearly Polarized Microstrip Antennas (From [Ref. 1]).....10
Figure 4. Various Type of Circularly Polarized Microstrip Patch Antennas: (a) Dual-Fed CP-Wave Patches; (b) Single Fed CP-Wave Patches (From [Ref. 2]).....12
Figure 5. Coordinate System and Angles for 3D Radiation Pattern 20
Figure 6. Polar Radiation Pattern Coordinate System and Angles.....21
Figure 7. The Receive (left) and the Transmit Antennas (right) for the Top Side.....22
Figure 8. The Receive (left) and the Transmit (right) Antennas for the Bottom Side 23
Figure 9. Transmit and Receive NPSAT1 Elliptical Microstrip Patch Antennas 24
Figure 10. Wire Frame Model of the Receive Antenna 25
Figure 11. Wire Frame Model of the Transmit Antenna.....26
Figure 12. Detailed View of the Receive Antenna [From NPSAT1 Design Team.] 27
Figure 13. Detailed View of the Transmit Antenna [From NPSAT1 Design Team.].....28
Figure 14. VSWR vs. Frequency for the Receive Antenna.....31
Figure 15. VSWR for Frequencies between 1.58 GHz and 1.775 GHz.....32
Figure 16. VSWR vs. Frequency for the Transmit Antenna 33
Figure 17. Detailed VSWR vs. Frequency between 2.038 GHz and 2.349 GHz.....33
Figure 18. Antenna Two-Port Reflection and Coupling Coefficients vs. Time.....34
Figure 19. Linear Scale Plots of Scattering Parameters vs. Frequency.....35
Figure 20. Logarithmic Scale Plots of Scattering Parameters (in dB) vs. Frequency.....36
Figure 21. Linear Scale Antenna Coupling Coefficient (S_{12} and S_{21}) vs. Frequency.....36
Figure 22. Logarithmic Scale Antenna Coupling Coefficient (S_{12} and S_{21} in dB) vs. Frequency.....37
Figure 23. S_{11} Smith Chart for the Receive Antenna.....38
Figure 24. S_{22} Smith Chart for the Transmit Antenna 38
Figure 25. 3-D Plot of Directivity at 1767.55 MHz 40
Figure 26. 3-D Plot of Left-Hand Circular Polarization at 1767.55 MHz 40
Figure 27. 3-D Plot of Right-Hand Circular Polarization at 1767.55 MHz 41
Figure 28. Polar Plot of Directivity as a Function of Theta for $\Phi = 0$, at 1767.55 MHz 42
Figure 29. Polar Plot of Directivity as a Function of Theta for $\Phi = 90$, at 1767.55 MHz 42
Figure 30. Polar Plot of LHCP at 1767.55 MHz.....43
Figure 31. Polar Plot of RHCP at 1767.55 MHz.....43
Figure 32. 3-D Plot of Directivity at 2207.3 MHz 44
Figure 33. 3-D Plot for LHCP at 2207.3 MHz.....45
Figure 34. 3-D Plot for RHCP at 2207.3 MHz.....45
Figure 35. Polar Plot of Directivity vs. Theta ($\Phi = 0$) at 2207.3 MHz.....46

Figure 36. Polar Plot of Directivity vs. Theta (Φ = 90) at 2207.3 MHz 46
Figure 37. Polar Plot of LHC at 2207.3 MHz 47
Figure 38. Polar Plot of RHC at 2207.3 MHz 47

LIST OF TABLES

Table 1. NPSAT1 and Antenna Coordinate System 19
Table 2. Axial Ratio Calculation for the Receive Antenna 48
Table 3. Axial Ratio Calculation for the Transmit Antenna 48
Table 4. Microwave Studio Solver Statistics 49

THIS PAGE INTENTIONALLY LEFT BLANK

ACKNOWLEDGMENTS

First of all, I would like to thank the United States government and the leadership of the Turkish Naval Forces for their trust and confidence in my abilities to allow me to study at one of the most prestigious institutions of learning in the world, the Naval Postgraduate School.

I also want to express my deepest appreciation to my dedicated and untiring thesis advisors, Professors Dr. Jovan Lebaric and Dr. Richard Adler of the Department of Electrical and Computer Engineering, for their expertise and precious time. I also thank them for teaching me the fundamentals of Electromagnetics. They have been exemplary advisors and scholars. I also want to thank Ron Russell for his help in editing my thesis.

I must also thank my dear wife, Esra, for being so patient and for carrying out every responsibility for care of our beloved newborn daughter, Ayse Ceyda. My wife's loving support during my research was priceless because of her unflagging belief in my abilities.

To all other friends and colleagues who contributed to this thesis in one way or another, I want to express my deepest appreciation and respect.

THIS PAGE INTENTIONALLY LEFT BLANK

EXECUTIVE SUMMARY

The aim of this research is to design a narrow-band antenna for the NPSAT1 space system, by using the CST Microwave Studio Finite Difference Time Domain (FDTD) software to develop, test, and analyze the RF propagation characteristics of the "elliptical patch" antenna and to determine the parameters that will give optimal results. The FDTD method uses approximate differential operators in Maxwell's equations. The most commonly used solution methods in the time domain are physical optics and the finite difference methods.

This thesis presents the design of two circularly polarized patch antennas for operation at 1.767 GHz and at 2.207 GHz, for receiving and transmitting, respectively. Additional design requirements for the NPSAT1 satellite antennas include a Voltage Standing Wave Ratio (VSWR) of less than or equal to 2:1 and 50 Ω input impedance. The study will also develop a three-dimensional antenna model that will be installed on the NPSAT1, whose main objective is to enhance the education of officer students at NPS.

The elliptical patch antenna is chosen for both the receive and transmit antenna, because of several advantages: it is lightweight, has small volume, has low profile planar configuration and has low fabrication cost. However, this approach has some disadvantages, such as narrow bandwidth, half plane radiation and a limitation on the maximum gain.

The polarization properties of an antenna should be matched to the fields radiated or received. The polarization of a receiving antenna must be matched to the polarization of the transmit antenna in order to extract maximum power from the field. If the antenna polarization is perpendicular to the received field polarization (such as vertical vs. horizontal, or right hand vs. left hand circular) the antenna will extract zero power.

Circularly polarized microstrip antennas (CP-MSAs) have recently received much attention and are used as efficient radiators in many communication systems. Therefore, in order to get the best performance regardless of the position of the NPSAT1, circular

polarization is chosen for this design. By properly adjusting the location of the single probe feed, one can create an elliptical patch antenna with good circular polarization.

The design process included the electromagnetic modeling and simulation, i.e., obtaining port signals, the S-Parameter plots, and the farfield pattern plots from the CST Microwave Studio FDTD software. The results of the simulation validated the initial design concept.

Through such simulation, the values of the axial ratio (representing the polarization quality for a circular polarized antenna) are found to be close enough to the 1.0 ideal value to ensure a good circular polarization. The VSWR of 2:1 is achieved from 1.5881 GHz to 1.7759 (187 MHz bandwidth) for the receive antenna, and from 2.038 GHz to 2.349 (310 MHz bandwidth) for the transmit antenna, thus meeting the requirements of the NPSAT1.

The performance of the proposed designs (in terms of input impedance and radiation patterns) does not change appreciably throughout the operating band. The maximum gain of the receive antenna is around 8.6 dBi with a side-lobe suppression of 11.6 dBi. For the transmit antenna the maximum gain is about 8.8 dBi with a side-lobe suppression of 15.7 dBi.

In conclusion, the simulations results presented in this study show that the proposed receive and transmit antennas are suitable for implementation as low cost, mechanically stable antennas with good circular polarization that satisfy the requirements of the NPSAT1.

Another student, Ltjg. Ilhan Gokben of the Turkish Navy, will use the optimized design resulting from this thesis to prototype and test the antennas that will eventually be installed on the NPSAT1.

I. INTRODUCTION

A. STATEMENT OF THE PROBLEM

1. Background

The primary goal for a microstrip patch antenna design is to determine the substrate and patch dimensions necessary to satisfy the required performance characteristics over the specified frequency band. The design procedure is initiated for the resonant frequency and the required radiation performance over the operational bandwidth via a step-by-step design process, as follows: Once the thickness and dielectric constant of the substrate have been chosen, based on material availability and requirements for space use, the approximate dimensions of a patch antenna are determined from the desired operating frequency and the known velocity of electromagnetic wave propagation in the patch substrate. The initial dimensions are then fine-tuned by an iterative procedure using computational electromagnetic software, preferably with a built-in optimizer, such as CST Microwave Studio. The design procedure is completed by finding a location of the feed point, such that the input impedance match to a 50 Ω reference yields a VSWR of less than or equal to 2:1.

The restrictions on antenna dimensions based on the available antenna "real-estate" on the NPSAT1 are for efficient operation at a VSWR specification of less than 2:1, and the 22-watt power handling capacity. These restrictions combine to limit the possible options to the use of microstrip patch antennas. This complicated problem would be very difficult to analyze and solve without using of computational electromagnetic tools (i.e., CAD software) and high-performance computer hardware.

2. Problem

This research addresses the following questions: (a) given the constraints on VSWR, bandwidth, physical dimensions and power handling capacity, what is the best antenna configuration to obtain optimal performance? and (b) what is the best available material to provide physical strength, while simultaneously satisfying the antenna VSWR requirements?

B. SCOPE AND LIMITATIONS

1. Scope

This study focuses on how to design one patch antenna for the receiver frequency of 1.767 GHz, and another for the transmit frequency of 2.207 GHz with a VSWR of less than or equal to 2:1 for a 50 Ω reference impedance. The study also includes: (a) the development of a three-dimensional antenna model for installation on the NPSAT1, (b) simulation of the RF excitation of the antenna and (c) analysis of the radiation patterns and the input impedance from the CST Microwave Studio Finite Difference Time Domain (FDTD) software package.

2. Limitations

This thesis will not cover the construction/fabrication of a prototype antenna. This research will not address the comparison of the measured results for antenna input impedances and radiation patterns with the predicted performance of the elliptical microstrip patch antenna models.

Ltjg. Ilhan Gokben of the Turkish Navy will use the optimized design resulting from this thesis to implement the prototype and test the antennas that will be installed on the NPSAT1.

C. OBJECTIVES OF THE STUDY

The objective of this thesis is to design two circularly polarized patch antennas for operation at 1.767 GHz and at 2.207 GHz, for receiving and transmitting respectively. Additional design requirements for the NPSAT1 satellite antennas include a VSWR of less than or equal to 2:1 and 50 Ω input impedance.

To accomplish the thesis objective, the CST Microwave Studio Finite Difference Time Domain (FDTD) software was used to develop, test, and analyze the RF characteristics of the elliptical microstrip patch antenna and to determine the antenna parameters for optimal performance. The basic geometry of a microstrip patch antenna consists of a conducting radiator patch printed onto a grounded substrate. Microstrip patch antennas make efficient radiators and are widely used in antenna applications.

D. BENEFIT OF THE STUDY

The study provides designs for low-profile receive and transmit patch antenna to be used aboard the NPSAT1. These designs will be implemented and tested in practice by Ltjg. Ilhan Gokben.

E. GENERAL BACKGROUND OF THE NPSAT1

1. Mission Objectives

A primary object of the NPSAT1 endeavor is to enhance the education of officer students at NPS. By providing hands-on engineering experience for an actual space system, officer students are exposed to the realities of systems engineering and the processes inherent in the flow from initial requirements to flight operations. From the standpoint of education, the spacecraft is a product of the educational process. The satellite itself will provide a test bed to demonstrate the technology of commercial, off-the-shelf (COTS) components for space applications. Furthermore it will provide an experimental platform for various scientific experiments.

2. Spacecraft Description

The NPSAT1 is an 81.6 kg [180 lb] satellite commissioned by the Department of Defense (DOD) Space Test Program (STP) MLV-05 Delta IV mission, due to launch in January 2006. The NPSAT1 is one of five secondary payloads that will participate in the Delta IV mission, using the Evolved Expendable Launch Vehicle (EELV) Secondary Payload Adapter (ESPA) 4. Figure 1 shows an expanded assembly drawing of the spacecraft, depicting modules located within the spacecraft. The overall configuration is shown in Figure 2, with the top, side, bottom, and isometric views shown. The spacecraft is a 12-sided cylinder with body-mounted solar cells on all of the cylinder sides. Both ends of the cylinder have antennas mounted on them to allow for communication in the event that the attitude of the spacecraft is not correctly nadir-pointing. This configuration assumes the risk, though remote, of an attitude control subsystem failure, combined with an attitude such that the cylinder's longitudinal axis points at the sun in either the plus or minus sense for an extended period of time, resulting in the loss of solar panel illumination. Two deployable booms are shown in Figure 2. These are the CERTO beacon

antennas and the Langmuir probe boom, respectively. The spacecraft subsystems include the Command and Data Handling (C&DH) subsystem, Electrical Power Subsystem (EPS), Attitude Control Subsystem (ACS), Radio Frequency Subsystem (RFS), and mechanical subsystems, which include the spacecraft structure, mechanisms, and thermal design. As a low-cost satellite, few space-rated components will be used, and the system will be a "single-string" design. The spacecraft's circular orbit with an altitude of 560 km and 35.4° inclination suggests a relatively radiation-benign environment.

As a result, the NPSAT1 has been designed, developed and integrated and will be tested completely at NPS facilities. Figure 3 shows the NPSAT1 existing structure and solar panels. After launch, it will be completely controlled by the NPS command station. NPSAT1 has been planned as a two-year mission life (minimum) and low-cost design (< $1M hardware cost) satellite. It will orbit the Earth at a height of 50-800 km, in a circular orbit with 30° to 80° inclinations. Some of the communication and physical features of the NPSAT1 are shown below:

- GMSK Modulation
- Full Duplex
- 100 kbps data rate
- Uplink at 1.767 GHz and Downlink at 2.207 GHz,
- Overall dimensions: 93 cm (37 in.) height x 50 cm (20 in.) diameter

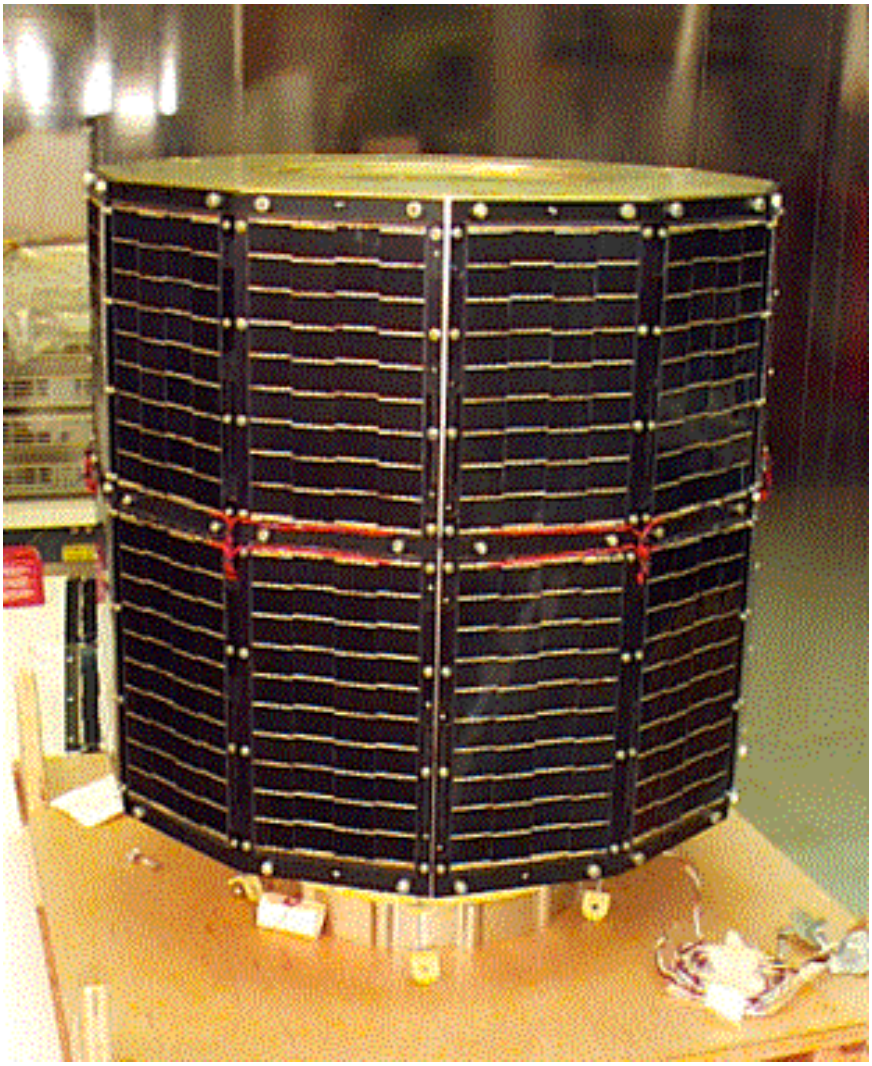

Figure 1. NPSAT1 Existing Structure and Solar Panels

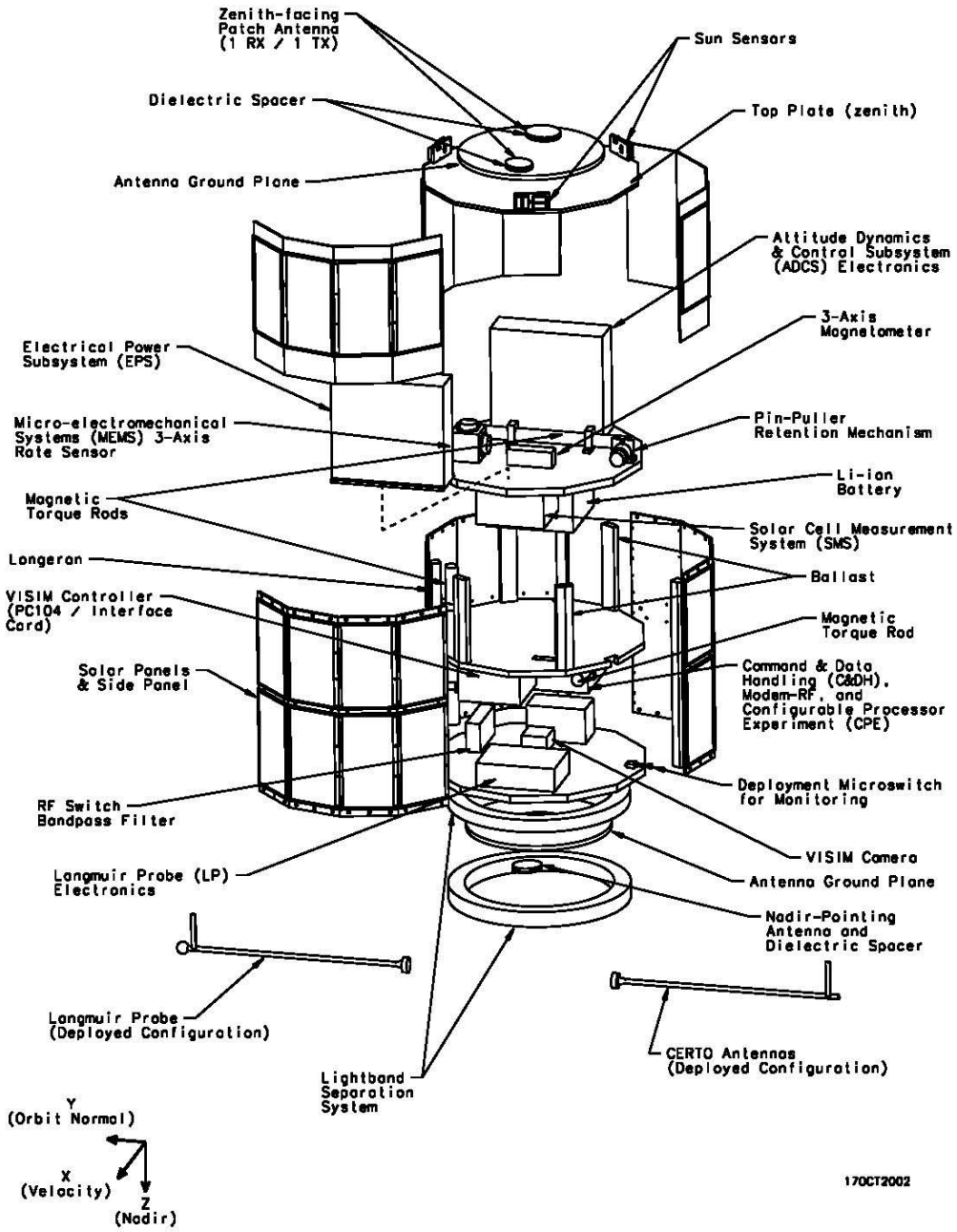

Figure 2. NPSAT1 Expanded View [From NPSAT1 Design Team.]

This thesis consists of five chapters. Chapter I introduces the research problem, the design of the receive and transmit patch antennas with a VSWR of less than or equal to 2:1 for a 50 Ω reference impedance, and presents some background information about the NPSAT1.

Chapter II briefly defines antenna polarization and shows how a microstrip antenna produces a circularly polarized (CP) wave.

Chapter III examines some of the most popular design techniques, particularly the FDTD method implemented in CST Microwave Studio, the computational electromagnetics software used in this study. This chapter also describes the procedure for choosing the structures and the dimensions of the proposed antenna.

Chapter IV presents the electromagnetic simulation results, i.e., port signals, S−parameter plots, and farfield patterns produced by CST Microwave Studio simulations to validate the patch antenna designs.

Finally, Chapter V presents conclusions and recommendations for possible continuation of this research.

THIS PAGE INTENTIONALLY LEFT BLANK

II. CIRCULARLY POLARIZED MICROSTRIP PATCH ANTENNAS

This Chapter briefly explains the definition of antenna polarization and demonstrates how a microstrip antenna produces a circularly polarized (CP) wave.

A. DEFINITION OF POLARIZATION

First the issue of antenna polarization is considered**.** At a large distance from a radiating antenna, the electric field vector of the radiated field is perpendicular to the direction of propagation. The polarization of an electromagnetic field is defined in terms of the direction of its electric field vector. If the electric field vector is always in one plane, then it is said to be linearly-polarized. Special cases are vertical polarization for the electric field vector in a vertical plane, and horizontal polarization for the electric field vector in a horizontal plane (typically with reference to the surface of the earth).

In general, the electric field vector rotates about a line parallel to the direction of propagation and its tip traces out an ellipse. This is known as elliptical polarization. Circular polarization (CP) is a special case of elliptical polarization in which the trace of the electric field vector is a circle. Because the electric field vector travels as a wave, the actual pattern is that of a spiral with an elliptical or circular cross section. The polarization of the receiving antenna must be matched to the polarization of the transmit antenna in order to extract maximum power from the field. If the antenna polarization is perpendicular to the field polarization (such as vertical vs. horizontal or right hand vs. left hand circular) the antenna will not extract any power from the incident wave.

B. CIRCULAR POLARIZATION FOR PATCH ANTENNAS

There are many types of linearly polarized microstrip patch antennas. In principle, the shape of patch is arbitrary, although square, rectangular, circular, ring, and elliptical designs are common, as shown in Figure 3, for linearly polarized microstrip antennas (MSAs). In Figure 3, typical locations of microstrip patch antenna feed points are indicated by an F (for “feed”). Although all of these antennas have very interesting

properties, the circularly polarized MSA designs used in this thesis have recently received increased attention and are used in many communication systems.

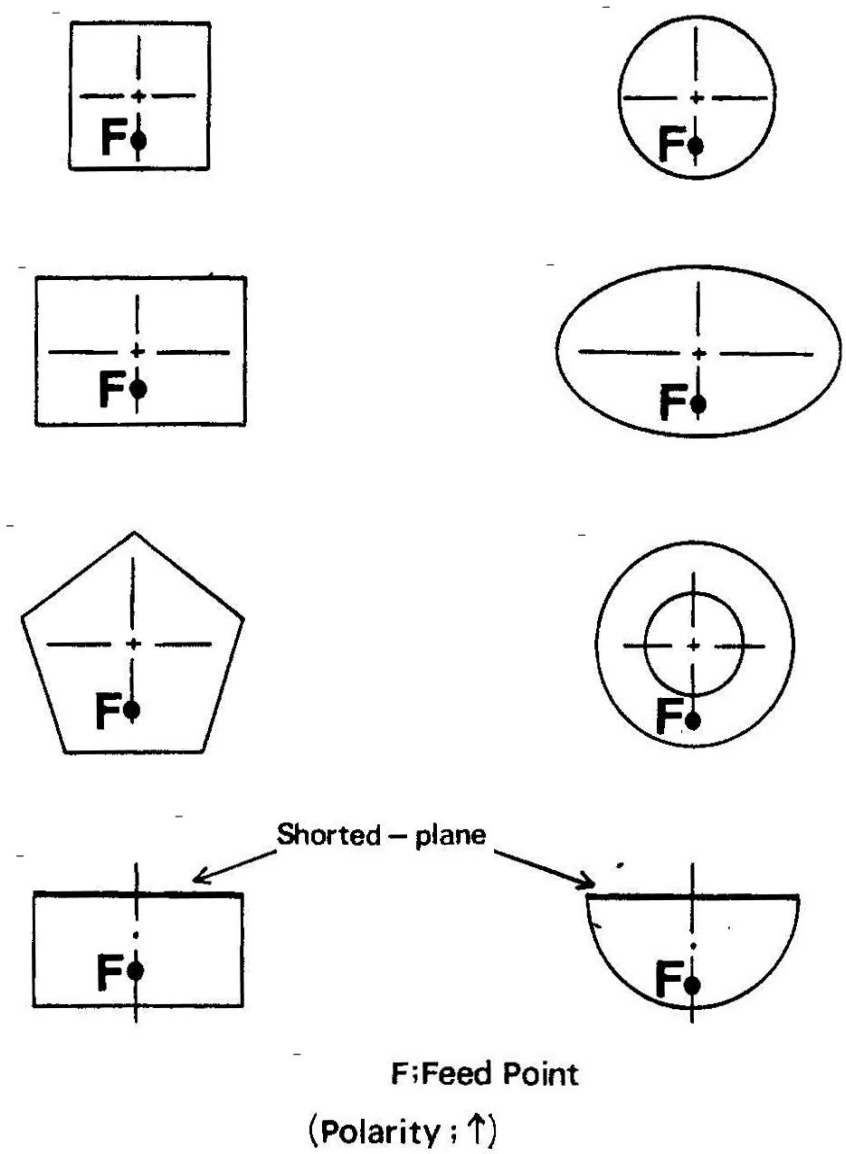

Figure 3. Basic Radiating Elements for Linearly Polarized Microstrip Antennas (From [Ref. 1])

In general, circularly polarized microstrip antennas can be categorized into two types according to the number of feed points: namely single-fed and dual-fed antennas. The basic configurations of a dual-fed CP antenna are illustrated in Figure 4 (a). Figure 4 (a) shows the antennas that are fed with an external polarizer, such as a 3 dB hybrid or offset feedline. In such an antenna system, the polarizer excites two linearly polarized orthogonal waves. The fields due to these orthogonal waves have equal amplitude and are 90° out of phase. Therefore, an antenna excited by an external polarizer acts as a CP-wave radiator. Both the impedance and axial ratio characteristics of dual-fed antennas are broader than those of single-fed antennas because the 3-dB hybrid is typically broadband.

On the other hand, single-fed circularly polarized patches are very attractive, because they can be arrayed and fed like any linearly polarized patch. The basic configurations of a single-fed antenna are shown in Figure 4 (b). Dual-fed CP patches require an additional circuit, which makes the overall size of the radiating element quite large, thus limiting the frequency performance of the array because of grating lobes. Single-fed CP patches have been extensively evaluated in the literature, where they are shown to be extremely narrowband antennas (1% bandwidth or less). The most frequently used types of single-fed circularly polarized patches are the slotted patch, the notched patch and the "almost square" patch.

In Figure 4 (b), Δs represents the size of the perturbation segment as shown at the edges of single-fed circularly-polarized MSAs and S denotes the area of the antenna. The two orthogonal ("degenerate") modes are separated into two modes by the effect of the perturbation segment Δs. The radiated fields caused by these two modes are perpendicular to each other and have equal amplitude, but are 90° out of phase if the size of the perturbation segment for an antenna is adjusted to the optimum. Therefore, a single-fed antenna with an optimum perturbation segment acts as a CP-wave radiator without using an external polarizer. Due to the perturbation, the patch surface currents in the x and y directions are simultaneously affected, which makes the manufacturing tolerance critical for CP operation. To avoid the need for fine tolerance, in this study the simple CP design technique was applied to single probe-feed elliptical microstrip antennas. In an elliptical microstrip patch antenna, the feed position is located along the 45º line between the long

and short axis of the elliptical patch, in order to simultaneously excite the two nearly degenerate modes corresponding to the long and short axes of the elliptical patch. The impedance matching is achieved by varying the feed position that is by moving the feed along the 45º line between the patch edge and the patch center.

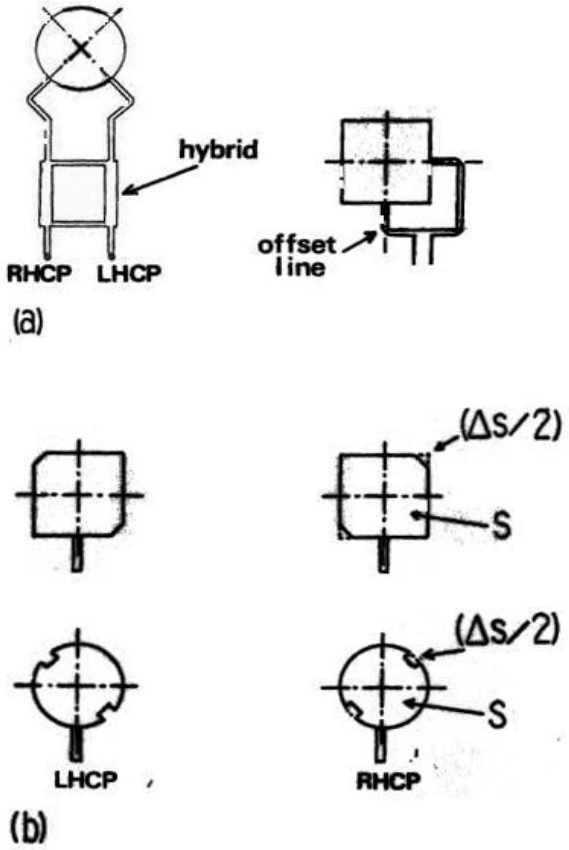

Figure 4. Various Type of Circularly Polarized Microstrip Patch Antennas: (a) Dual-Fed CP-Wave Patches; (b) Single Fed CP-Wave Patches (From [Ref. 2])

This Chapter presented design options for circularly polarized microstrip patch antennas. The particular design selected for the NPSAT1 is a single-feed microstrip elliptical patch antenna, because of its ease of fabrication and good electrical and mechanical performance. By proper adjustment of the location of the single probe feed, right-

hand or left-hand CP radiation can be obtained and the impedance can be matched to the 50 Ω reference.

The following chapter presents the FDTD technique used in this project, and also describes the procedure used for determining the antenna dimensions needed to meet the NPSAT1 antenna requirements.

THIS PAGE INTENTIONALLY LEFT BLANK

III. DESIGN OF THE ANTENNA AND COMPONENTS

This Chapter examines several popular design techniques, including the FDTD (Finite Difference Time Domain) technique, used in this project. This chapter also describes the procedure for choosing the structures and the dimensions of the proposed antenna, such that antenna input impedances meets the VSWR requirement of the NPSAT1.

A. DESIGN METHODOLOGY

1. Design Techniques and Software

The microstrip patch antenna has been analyzed using different techniques:

- Transmission Line Model [Ref. 3]
- Cavity Model [Ref. 4]
- Methods of Moments [Ref. 5]
- Finite-difference Time-domain Method [Ref. 6]

In the transmission line model, the patch antenna is treated as two parallel radiating slots connected by a transmission line. The length of the patch antenna in the model is assumed larger than the actual physical length, to account for the fringing effect on the edges of the patch. Although the transmission-line model is easy to use, it has some inherent disadvantages. Specifically, it is only useful for patches of rectangular (or square) design and it inherently ignores details of field variations along the radiating edges. Employing the cavity model can overcome some of these disadvantages.

Calculations based on the cavity model are the most useful for analyzing patch antennas. The cavity model treats the region between the two parallel conductor planes, consisting of a patch radiator and ground plane, as a cavity bounded by electric walls and a magnetic wall along the periphery of the patch. The antenna fields are assumed to be those of this cavity. Once the field distribution has been determined for the cavity, Huygens' principle may be applied to the magnetic wall of the cavity, and then the approximate radiation field can be evaluated. This method is the most suitable for

analyzing patch antennas whose geometries and the corresponding wave equation for the cavity model can be solved by employing the method of separation of variables.

Microstrip antennas are often used in conformal arrays because of their ability to conform to non-planar structures. Algorithms and software have been developed for analyzing different configurations of rectangular microstrip patch antenna arrays based on the Method of Moments approach. Input impedance, mutual coupling and radiation patterns are calculated and results are validated against measurements on an experimental model. While the Method of Moments is general, it requires considerable computational effort and yields few physical insights. The cavity model offers both simplicity and physical insight. [Ref. 7]

This thesis uses FDTD technique, specifically the CST Microwave Studio FDTD software. The FDTD method applies approximate differential operators to discretize Maxwell's equations. The spatial and time derivatives in Maxwell's equations are approximated by finite differences. The FDTD technique has the advantage of being able to analyze structures with arbitrary shapes and a wide variety of materials. Each volumetric cell in FDTD can have a permittivity and permeability independent of all other cells.

With this approach, the incident plane wave must be introduced into the grid and propagated to the target in discrete steps. The scattered field must exit the grid without introducing artificial reflections. A perfectly matched layer (PML) boundary is commonly used at the grid boundary; large grids can be used so that the residual reflections from the grid boundary occur late in time and can be filtered out. For stability, Courant conditions must be satisfied, linking the cell size (spatial disretization) and the discrete time steps. The FDTD is convenient for very broadband excitations, as solutions at multiple frequencies are obtained via a single time domain calculation. The Fourier Transform of time-sampled scattered waveforms provides the required parameters over a wide bandwidth.

The CST Microwave Studio is a specialized tool for fast and accurate three-dimensional electromagnetic simulation of high-frequency problems. It has electrostatics

and magnetostatic solvers, is fully parameterized, and possesses other key features, such as VBA compatibility, automatic macro recording, automatic multi-dimensional parameter sweeps and optimizers. Modeling with CST allows the use of an interactive mouse for data input, design capture, template assistance for specific applications, and fully parametric 3D modeling. A "history list" permits unlimited "undo" and "redo" functions for editing. The software also has advanced solid modeling features, including helices, blends, chamfers, extrusions, lofting and Boolean operations such as adding and subtracting solid objects from existing structures. Additionally, it allows the import of 3D and planar structures and the parameterization of imported objects.

The software provides automatic meshing and adaptive mesh refinement options. Simulation materials can be arranged in layers, whether they are isotropic or anisotropic, linear or non-linear, magnetic or non-magnetic. RF energy excitation sources include waveguide ports, plane wave incident fields, and discrete voltage and current sources. The post-processing includes the VSWR and Smith chart plots, port signal plots, polar radiation pattern plots, and 2D and 3D field plots. The software can also calculate and plot the antenna axial ratio, which is important for circularly and elliptically polarized antennas.

The first step in the antenna design processes is determining the criteria to use in selecting an optimal antenna. The first criterion is to achieve power transfer from the feed transmission line to the antenna. This is accomplished by the matching the antenna input impedance to the characteristic impedance of the transmission line (in our case a coaxial cable with a $50\,\Omega$ characteristic impedance). Ulaby [Ref. 8] defines these relations by the following equations:

$$\Gamma = \frac{Z_L - 50}{Z_L + 50} = \frac{VSWR - 1}{VSWR + 1} \tag{1}$$

$$VSWR = \frac{1 + \Gamma}{1 - \Gamma} \tag{2}$$

$$\text{Mismatch Loss (dB)} = -10\log_{10}[1 - |\Gamma|^2]. \tag{3}$$

In order to achieve the minimum acceptable *VSWR* of 2:1, the reflection coefficient must be $\Gamma = 0.333$, a corresponding load impedance of $Z_L = 100$ ohms and transmission line impedance of $Z_0 = 50\ \Omega$, where

$$Z_L = (-50) \cdot \frac{\Gamma + 1}{\Gamma - 1}. \tag{4}$$

Another major criterion in selecting an antenna is its overall efficiency, the product of the input efficiency, radiation efficiency and beam efficiency, and is expressed by the relation:

$$\eta_{overall} = \eta_{input} \cdot \eta_{rad} \cdot \eta_{beam}. \tag{5}$$

Input efficiency defines the fraction of input power that effectively couples source power to the antenna and is computed using the formula:

$$\eta_{input} = 1 - |\Gamma|^2 \tag{6}$$

where Γ is the reflection coefficient or S_{11} defined by:

$$\Gamma = \frac{Z_{in} - Z_{ref}}{Z_{in} + Z_{ref}}. \tag{7}$$

The CST Microwave Studio software designates the reflection coefficient as the S_{11} parameter. The radiation efficiency provides the portion of coupled power that the antenna radiates, and is expressed as a ratio of radiated power to input power. In equation form:

$$\eta_{rad} = \frac{P_{rad}}{P_{in}} = \frac{R_{rad}}{R_{rad} + R_L} \tag{8}$$

where R_{rad} is the effective radiation resistance and R_L is the antenna loss resistance.

If the radiation resistance is small compared to the loss resistance, the antenna radiation efficiency is low. For electrically small antennas, the radiation resistance varies as approximately $(L/\lambda)^2$ for an electrically small loop, and approximately as L/λ^4 for

an electrically short dipole, where L is the antenna length and λ is the wavelength at the frequency of operation.

Beam efficiency provides the fraction of the total radiated power, at the desired polarization, into the desired target space volume. The total radiated power can be calculated as the product of the input power and the antenna average gain. The total power efficiency is frequency dependent for most antennas, but this dependence can be removed by averaging the overall efficiency over the operating frequency range. The optimal antenna should have the highest mean efficiency with the least variance of the efficiency over the intended operational frequency range.

2. NPSAT1 Relative Position and Coordinate System Used

In order to define a solid 3D structure in any computer-aided-design software, operations are performed in a particular global and/or local co-ordinate system. To clarify these, Table 1 designates the transverse axes of the three-dimensional drawings, and angles for the radiation pattern plots, relative to the NPSAT1 flight path.

AXIS OR ANGLE	INTERPRETATION
X-axis	Direction of the satellite flight
Y-axis	Perpendicular to the direction of the satellite flight
Z-axis	Direction pointing toward the earth
Phi (Φ) = Satellite Yaw Angle	$\Phi = 0^o$ points to direction of satellite's head or direction of flight $\Phi = \pm 90^o$ points outward from satellite along the horizontal or X-Y plane.
Theta (θ) = Satellite Angle of Radiation	$\theta = 0^o$ points toward the ground $\theta = 90^o$ lies along the horizontal plane parallel to the ground $\theta = 180^o$ points toward the zenith or the sun at noon time

Table 1. NPSAT1 and Antenna Coordinate System

The CST Microwave Studio software uses the fixed global xyz-coordinate system. The farfield is represented by two components $(E_{\grave{e}}, E_{\ddot{o}})$ at spherical coordinates theta (θ) and phi (ϕ). The coordinates theta and phi relate to the Cartesian coordinate system as shown in Figure 5. The angle phi is defined in the XY-plane, measured counter-clockwise from the X-axis, and the angle theta is denoted in the XZ-plane, measured clockwise from the Z-axis. Figure 6 presents the far-field polar plot with one spherical coordinate (theta) varying, and the other (phi) fixed.

Figure 6 shows a cut plot of the 3D radiation pattern for $\Phi = 90$. The zenith direction coincides with $\theta = 0$ axis (horizontal). The counter-clockwise direction from the $\theta = 0$ axis is towards the positive x-axis, as indicated by the $\Phi = 90$ label, while the clockwise direction from the $\theta = 0$ axis is towards the negative x-axis, as indicated by the $\Phi = 270$ label.

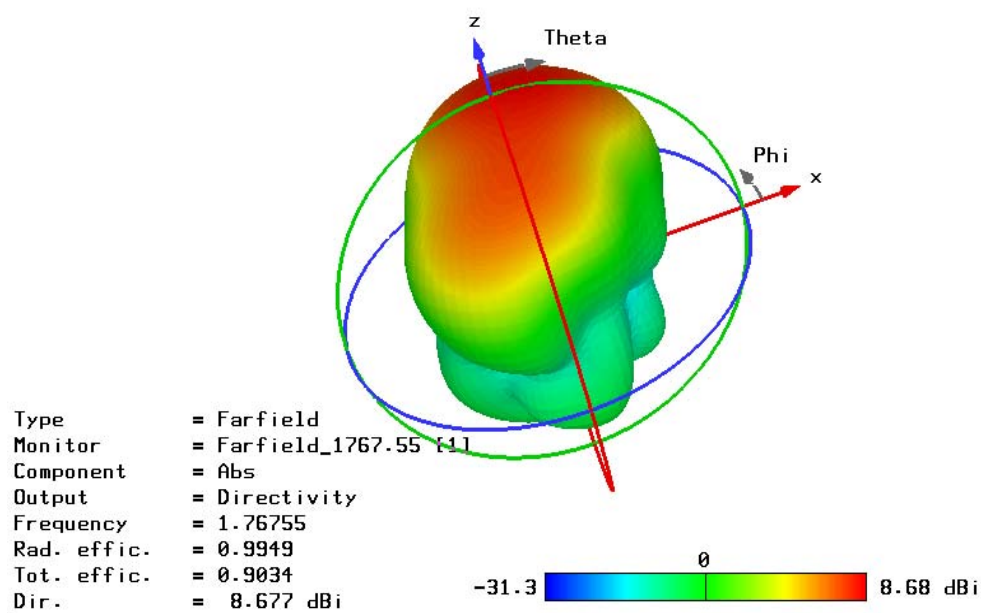

Figure 5. Coordinate System and Angles for 3D Radiation Pattern

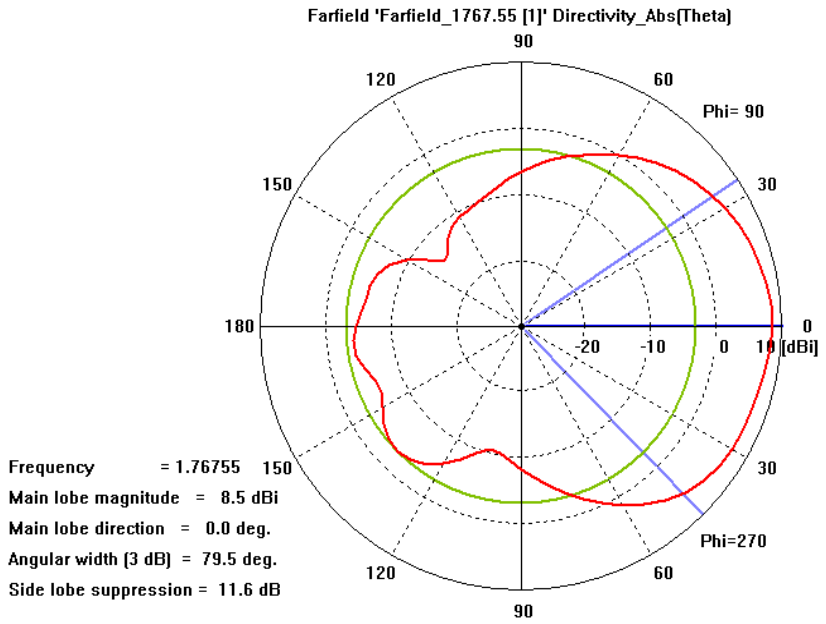

Figure 6. Polar Radiation Pattern Coordinate System and Angles

B. GENERAL DESCRIPTION OF THE ANTENNA ASSEMBLY

The proposed antenna consists of a metallic "elliptical patch" on a dielectric (Teflon) substrate. Due to strict dimension restrictions the antenna must not exceed 10 centimeters on the larger axis of the elliptical shape. The antenna has a band of operation from 1.5881 GHz to 1.7759 GHZ (187 MHz bandwidth) as a receive antenna, from 2.039 GHz to 2.349 GHz (310 MHz bandwidth) as a transmit antenna, and a VSWR of 2:1 or lower. An overview of various references in the antenna area revealed no "ready-made" formulas for designing of an "elliptical microstrip patch" antenna with dimensional restrictions and specific electrical performance requirements.

A microstrip patch antenna is composed of three layers: a ground plane, a dielectric substrate layer, and a patch. The patch is connected with an RF source through a coaxial line feed or a microstrip line feed. Since the patch is a perfect conductor, there is no tangential electric field on its surface. Furthermore, though the patch is open circuited at the edges, it is not a perfect open circuit since the dielectric substrate is very thin compared to the wavelength at the operating frequency. For the above reason, the fringing electric fields appear on the edges of the patch. Thus, the radiation aperture is larger than the physical aperture.

Techniques for feeding patches are summarized into three groups: direct feed coupled, electromagnetically coupled, or aperture coupled. Direct coupling methods are the oldest and the most popular, but only provide one degree of freedom for adjusting impedance. The microstrip feed-line and the coaxial probe are examples of direct feeds. The direct coaxial probe feed is simple to implement by extending the center conductor of the connector, attached to the ground plane, up (through the substrate) to the patch. The impedance can be adjusted by proper placement of the probe feed relative to the patch center. As the probe distance from the patch edge increases, the input impedance is, in general, reduced. A disadvantage of the probe feed is that it introduces an inductance that prevents the patch from becoming resonant, if the thickness of the substrate is 0.1 λ or greater. Also, probe radiation can be a source of cross polarization. [Ref. 9]

Figures 7 and 8 illustrate a three-dimensional broadside model of the elliptical patch antennas proposed for the NPSAT1, installed on the top and the bottom sides of the satellite.

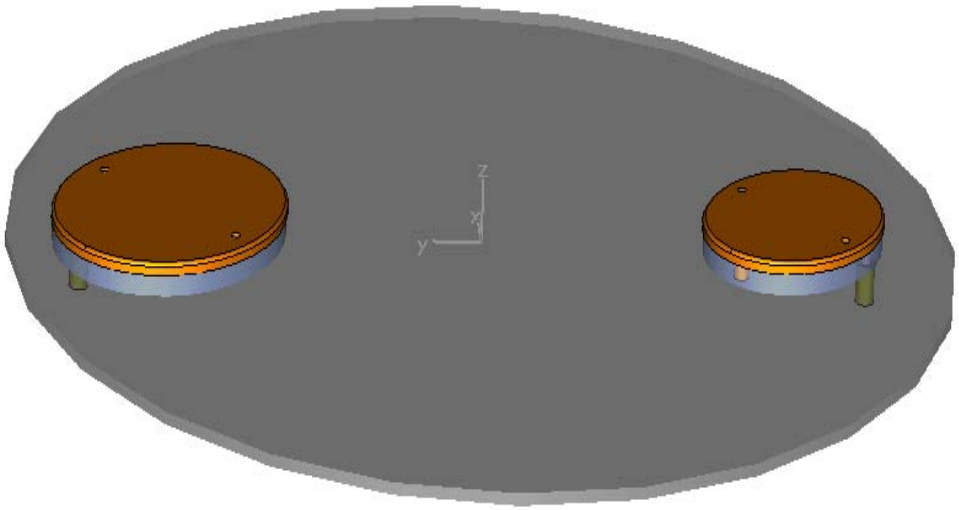

Figure 7. The Receive (left) and the Transmit Antennas (right) for the Top Side

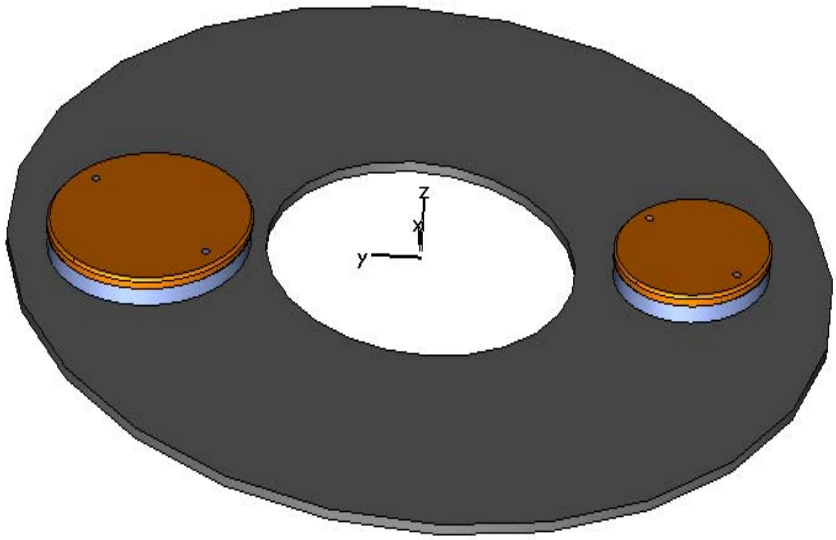

Figure 8. The Receive (left) and the Transmit (right) Antennas for the Bottom Side

Figure 9 shows the 3D models of the transmit microstrip patch antenna and the receive microstrip patch, viewed from the YZ plane. Note that the simulations used a flat circular ground-plane corresponding to the metallic surface, visible in Figure 9, to which the antenna substrate is attached.

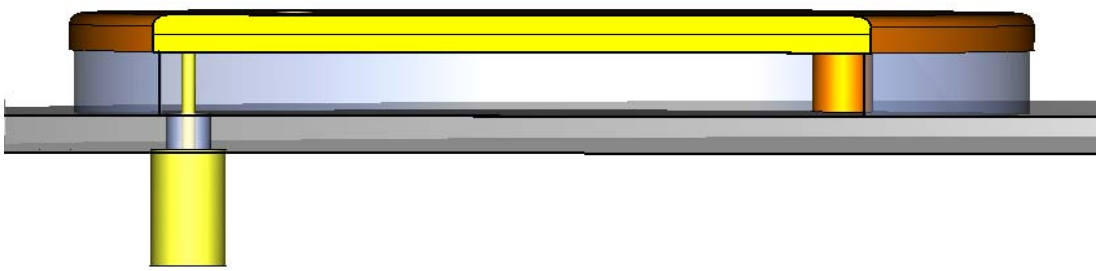

(a) The Model of the Receive Antenna, YZ-Plane

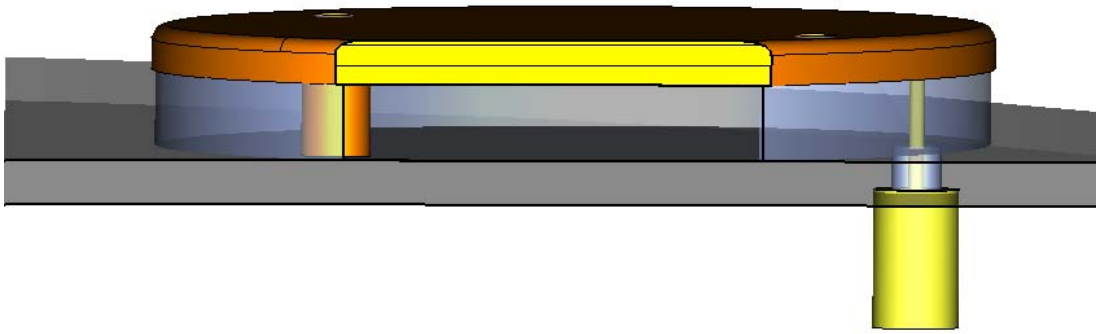

(b) The Model of the Transmit Antenna, YZ-Plane

Figure 9. Transmit and Receive NPSAT1 Elliptical Microstrip Patch Antennas

Figure 10 and 11 show the specifications of the materials and their associated positions on the 3D antenna model, by using a wire frame drawing in CST Microwave Studio.

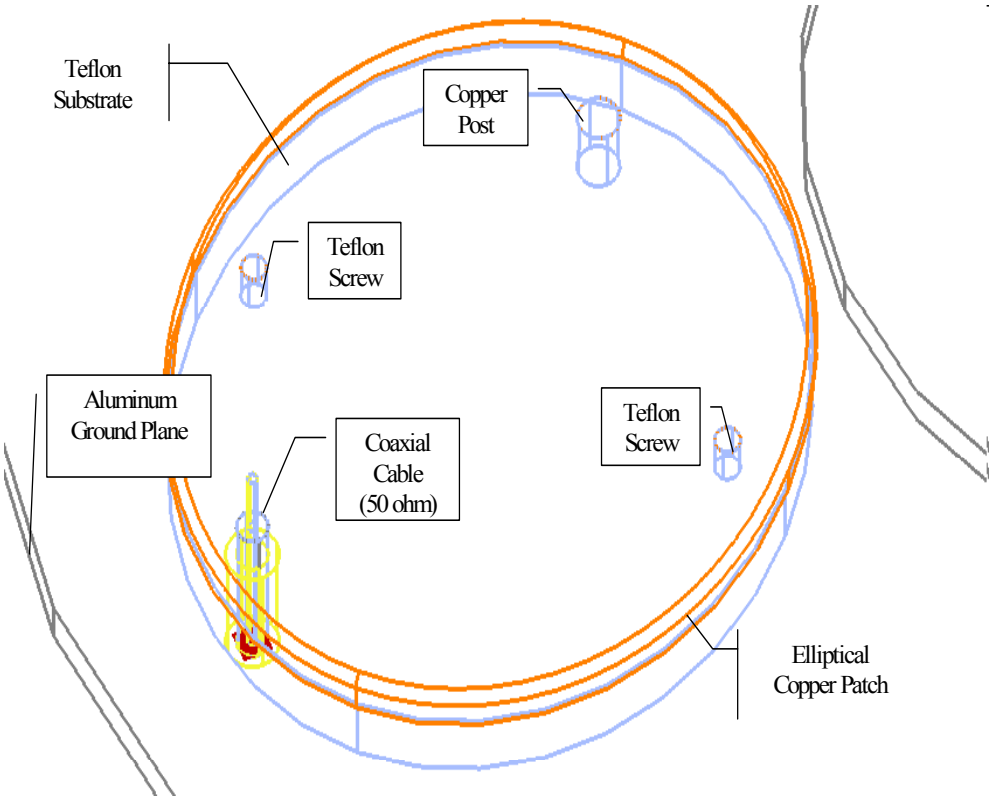

Figure 10. Wire Frame Model of the Receive Antenna

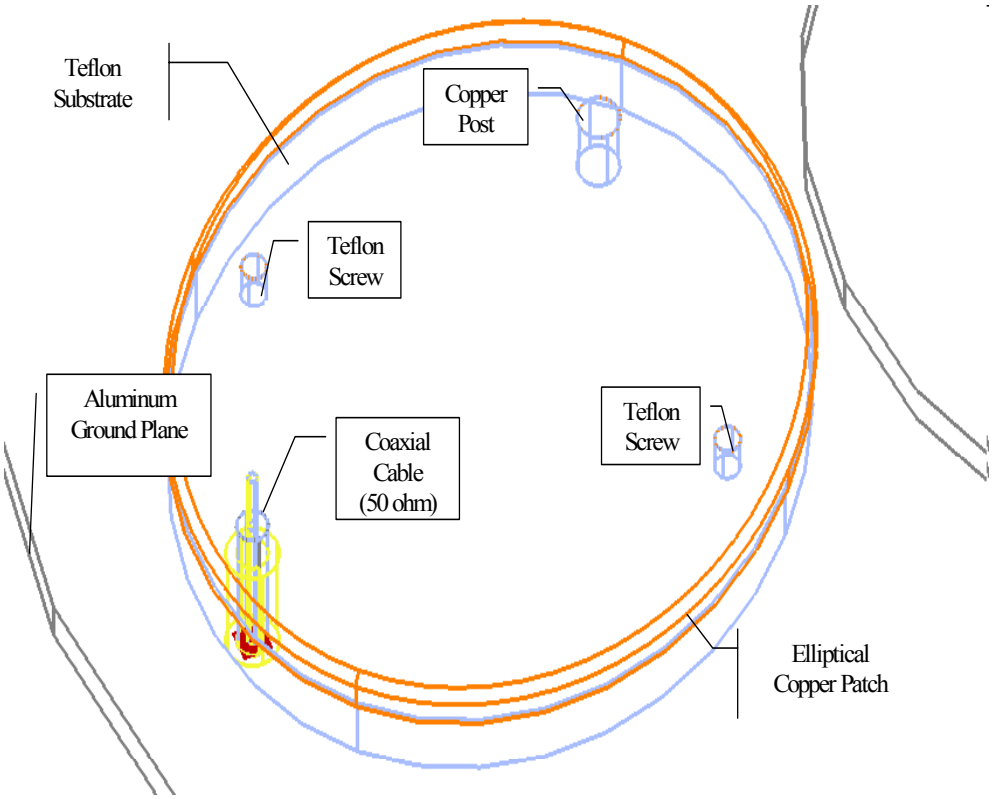

Figure 11. Wire Frame Model of the Transmit Antenna

Figures 12 and 13 present detailed views of the receive patch antenna and the transmit patch antenna. The physical dimensions of the two antennas are shown in Appendixes A and B, respectively.

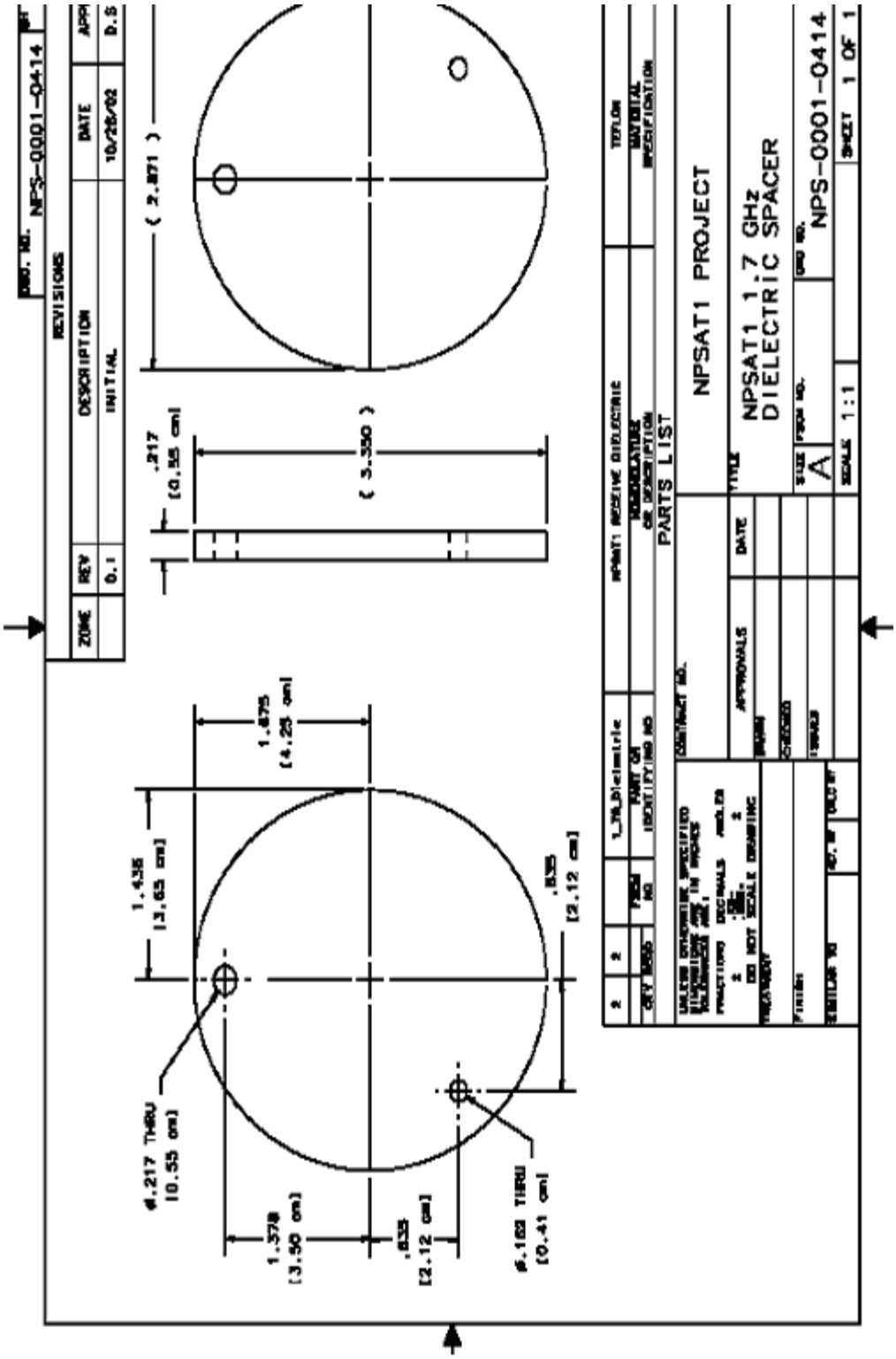

Figure 12. Detailed View of the Receive Antenna [From NPSAT1 Design Team.]

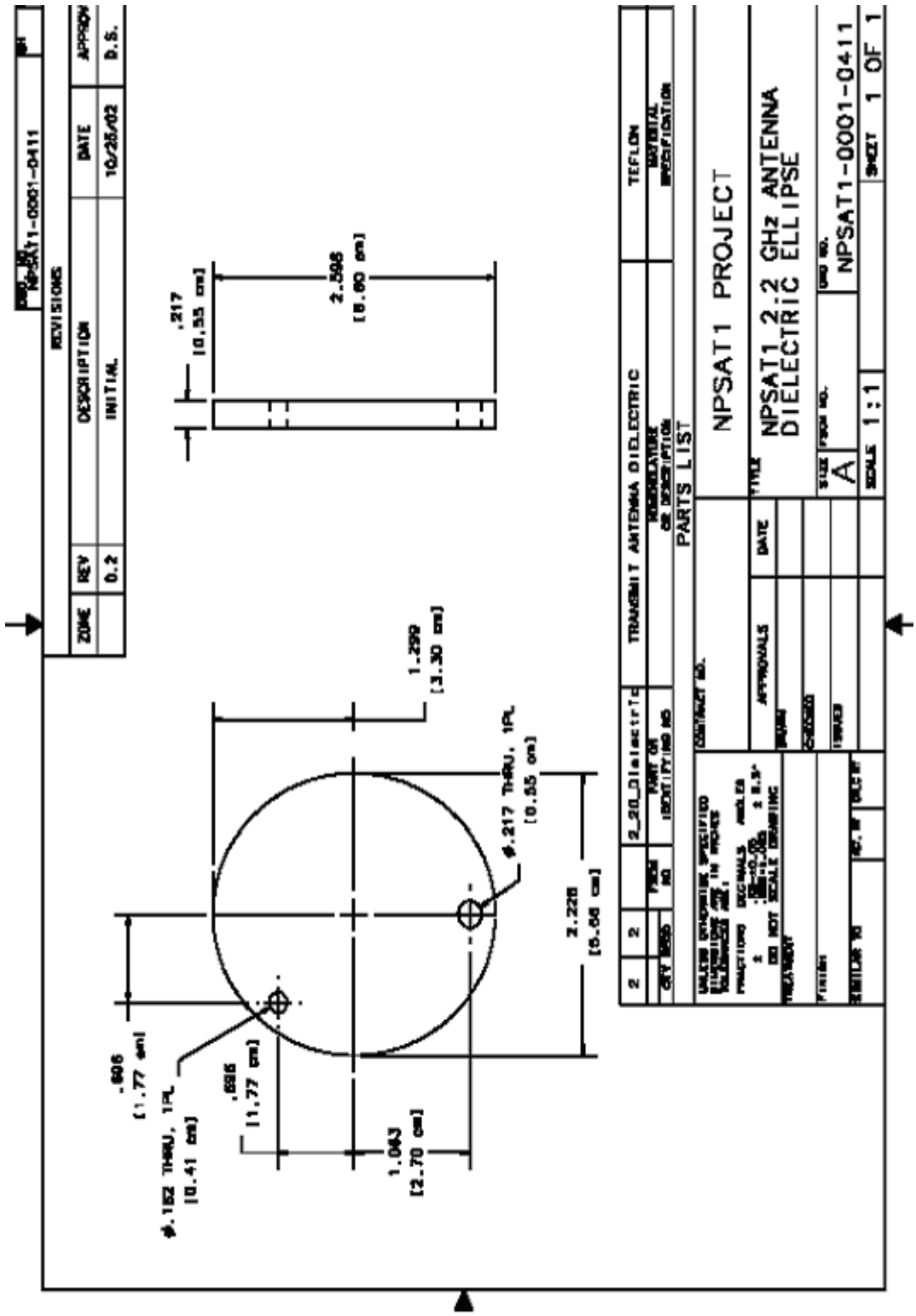

Figure 13. Detailed View of the Transmit Antenna [From NPSAT1 Design Team.]

This Chapter examined some of the most popular computer-based design techniques, particularly the FDTD method implemented in the CST Microwave Studio software used in this study. The proposed microstrip patch antenna structures have been shown to satisfy the NPSAT1 requirements with respect to the available antenna "real estate" and mechanical stability. Chapter IV presents the electromagnetic simulation results, using CST Microwave Studio FDTD software to validate the electrical performance of the two proposed patch antennas.

THIS PAGE INTENTIONALLY LEFT BLANK

IV. ELECTROMAGNETIC SIMULATION RESULTS

This Chapter presents the electromagnetic simulation results that were obtained by using CST Microwave Studio FDTD software to validate the electrical performance of the proposed microstrip patch antennas. CST Microwave Studio allows calculation and plotting different quantities in the time and frequency domains, such as VSWR vs. frequency, port time-domain signals, the S-parameter plots, and so on. In addition to these one-dimensional (1D) plots, CST Microwave Studio post-processing also includes visualization of many different 2D and three 3D quantities, such as electric and magnetic vector and scalar fields, power flow, and volumetric radiation patterns.

A. VSWR AS A FUNCTION OF FREQUENCY

1. VSWR for the Receive Antenna

Figure 14 shows the VSWR for the elliptical microstrip receive patch antenna, for frequencies up to 5 GHz.

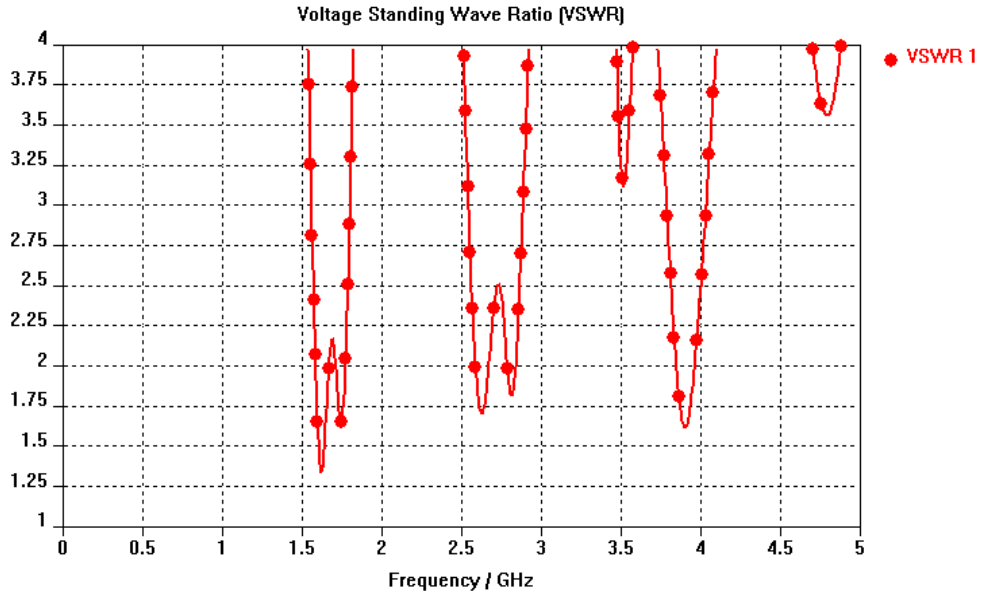

Figure 14. VSWR vs. Frequency for the Receive Antenna

Figure 14 also shows that the antenna operates well in two additional bands: from 2.6 GHz to 2.85 GHz (250 MHz bandwidth), and from 3.84 GHz to 3.96 (122 MHz bandwidth), but these are bands outside the NPSAT1 antenna operational frequency range, and will be suppressed by the receiving bandpass filter which is a part of the receiver RF front-end. Figure 15 presents the detailed VSWR vs. frequency from 1.58 GHz to 1.775 GHz, illustrating that a VSWR of less than 2.2:1 is achieved from 1.5881 GHz to 1.7759 (187 MHz bandwidth).

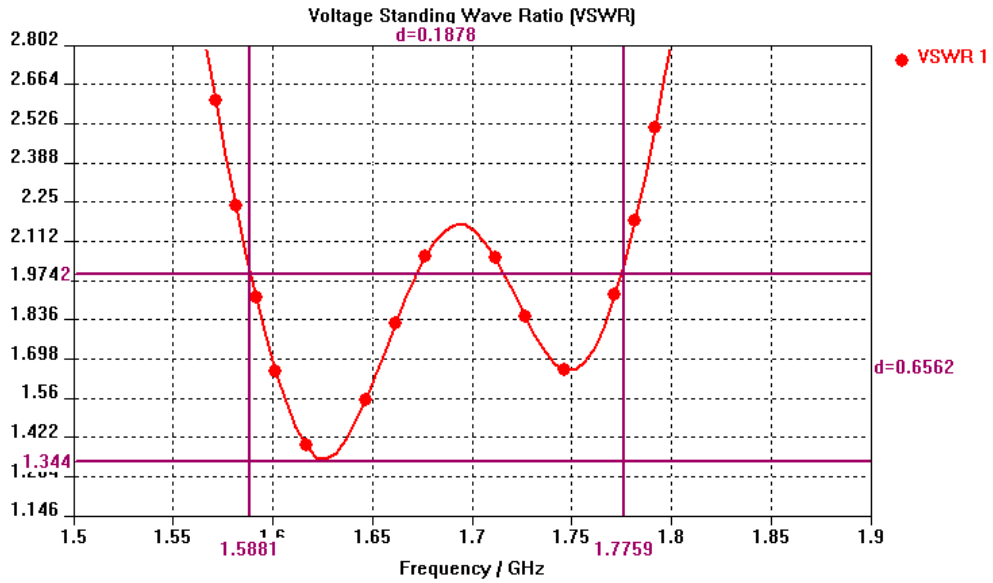

Figure 15. VSWR for Frequencies between 1.58 GHz and 1.775 GHz

2. VSWR for the Transmit Antenna

Figure 16 shows the VSWR for the NPSAT1 elliptical microstrip patch transmit antenna, at frequencies up to 5 GHz. Figure 17 presents the detailed VSWR vs. frequency from 2.038 GHz to 2.349 GHz. A VSWR of less than 2.2:1 is achieved from 2.039 GHz to 2.349 (310 MHz bandwidth) and from 3.34 GHz to 3.74 GHz (400 MHz bandwidth). The second band is well outside of the operating frequency range of the NPSAT1 transmitter and has no adverse effects on the overall system operation.

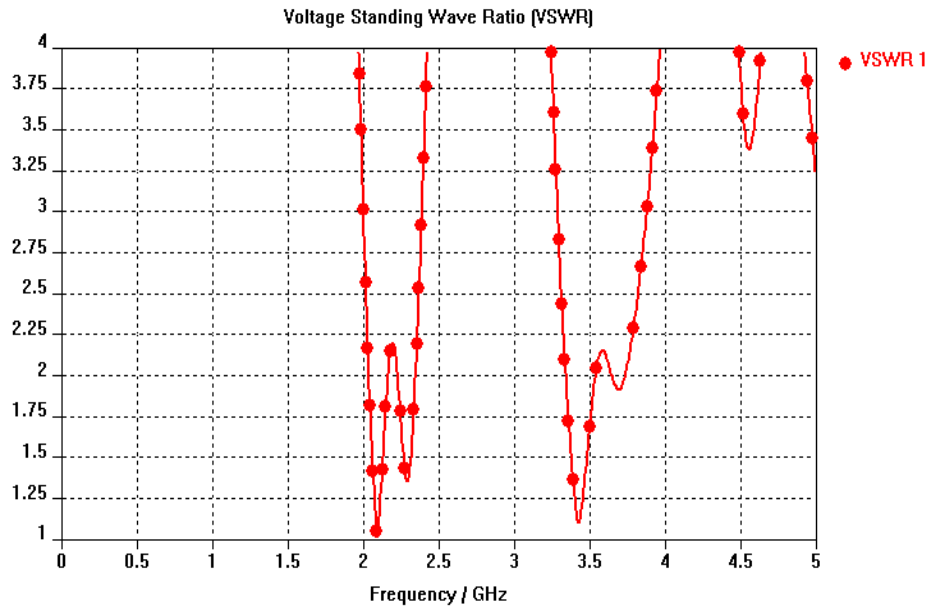

Figure 16. VSWR vs. Frequency for the Transmit Antenna

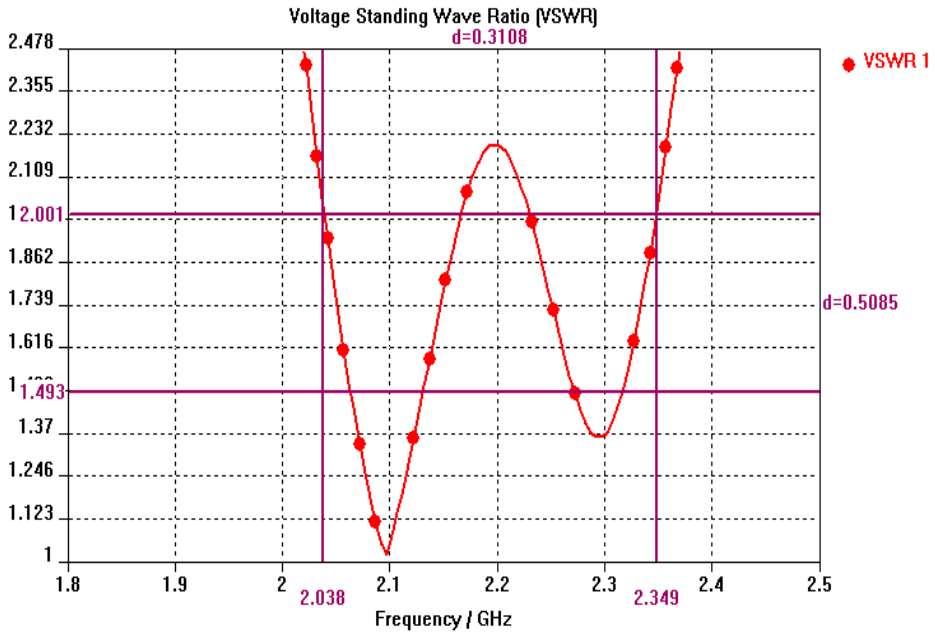

Figure 17. Detailed VSWR vs. Frequency between 2.038 GHz and 2.349 GHz

3. Port Signals

Figure 18 shows the incoming and outgoing time-domain waveforms for the two-port formed by the transmit antenna and the receive antenna coaxial feed ports. Port 1 and Port 2 refer to the feed ports of the receive antenna and the transmit antenna respectively. The incident wave amplitudes are denoted i_1 and i_2 and the output wave amplitudes for the two ports are denoted o_{11}, o_{21}, o_{12} and o_{22}. The output wave amplitudes o_{21} and o_{12} are identical and appear as a single curve, because the two-port is reciprocal. The antenna-to-antenna coupling is very weak and thus the o_{21} and o_{12} curves appear to be right on the horizontal (zero amplitude) axis. The patch antennas have strong resonances that lead to a slowly decaying output (reflected) signals.

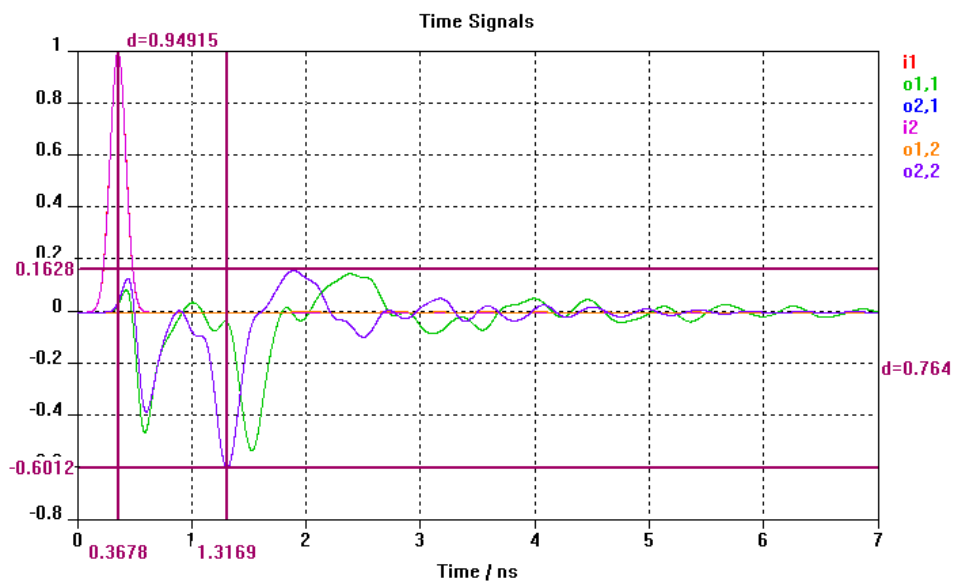

Figure 18. Antenna Two-Port Reflection and Coupling Coefficients vs. Time

4. S- Parameters

One of the primary results from the antenna simulations are the S-parameter (magnitude and phase) plots versus frequency. The S-Parameters plot show resonance frequencies and operating bandwidths for the microstrip patch antennas analyzed.

a. S-Parameter Magnitude

Figures 19 and 20 show the *S*-parameters (reflection coefficients and coupling coefficients) for the two-port formed by the transmit antenna (magenta curves) and the receive antenna (red curves). Figure 19 shows the reflection and coupling coefficients on a linear scale, and Figure 20 shows the reflection and coupling coefficients on a logarithmic scale, for increased dynamic range. Note that the two antennas are coupled electromagnetically, albeit very weakly. The frequencies of efficient antenna operation are indicated by the minima of the reflection coefficients. So, we can identify the microstrip patch antenna resonant frequencies of 1.767 GHz for the receive antenna and 2.207 GHz for the transmit antenna, which closely matches the NPSAT1 requirements. Figures 19 and 20 also show the mutual coupling coefficients represented by the blue and the green lines, which are identical because of the antenna two-port reciprocity. Note that the logarithmic scale in Figure 20 allows much better quantification of the very weak coupling between the two antennas.

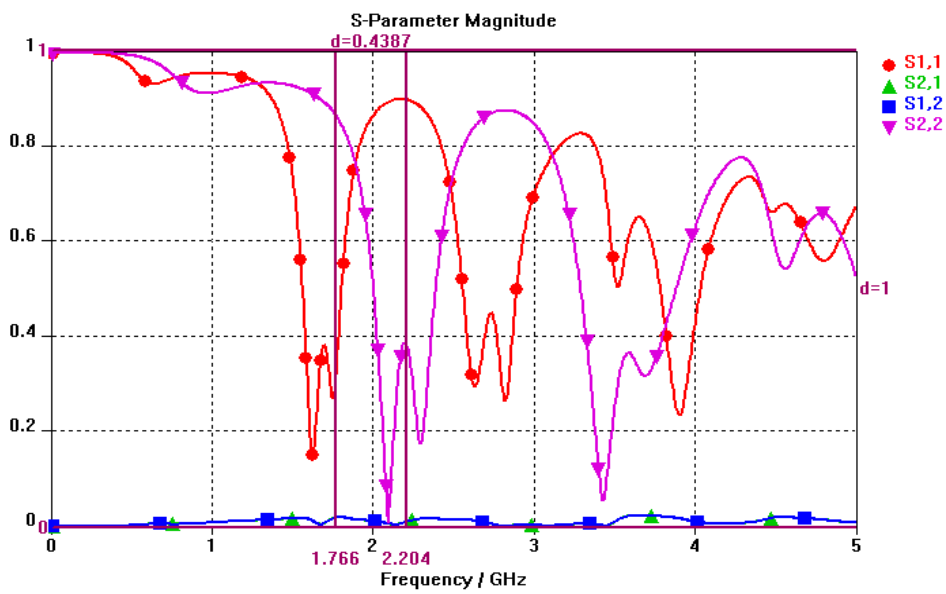

Figure 19. Linear Scale Plots of Scattering Parameters vs. Frequency

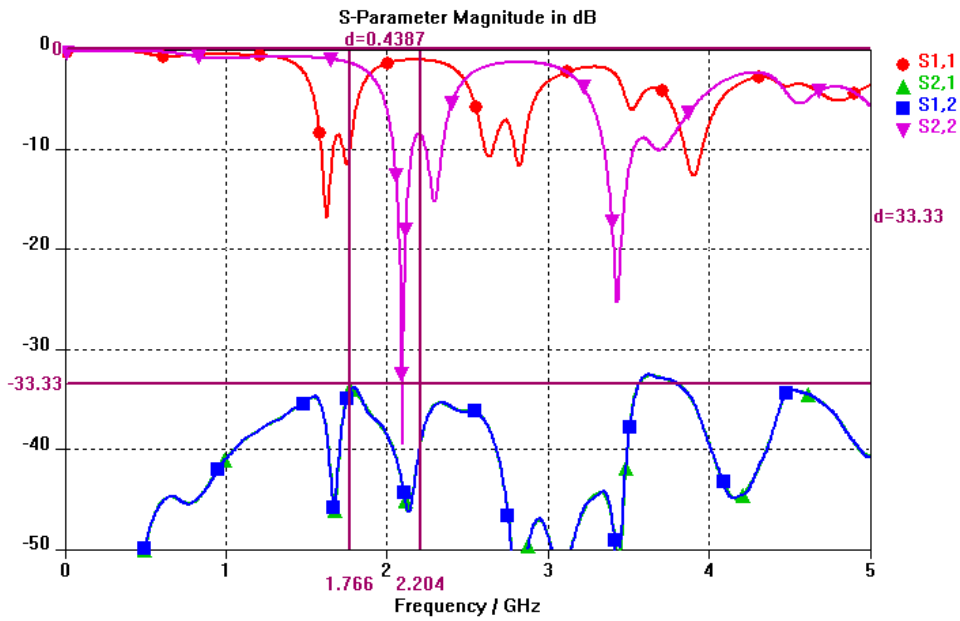

Figure 20. Logarithmic Scale Plots of Scattering Parameters (in dB) vs. Frequency

b. Mutual Coupling S-Parameter Magnitude

Figures 21 and 22 emphasize *S*-parameter plots for the mutual coupling between the transmit antenna and the receive antenna (S_{12} and S_{21}).

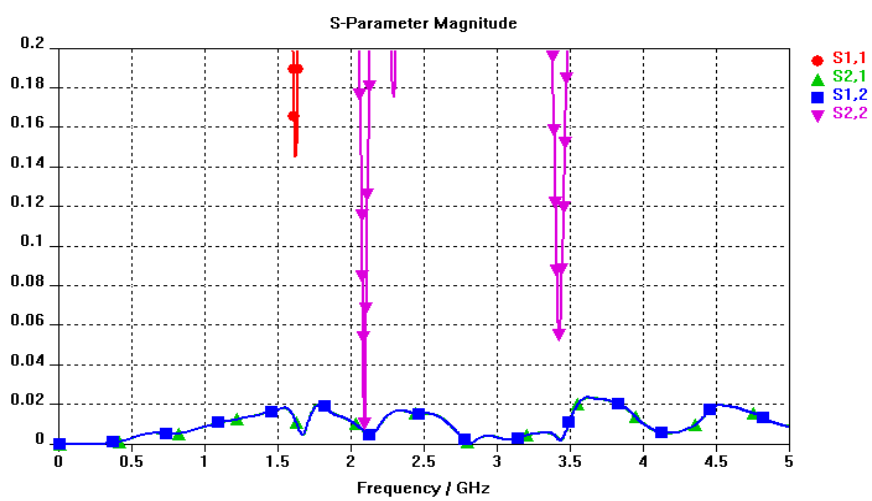

Figure 21. Linear Scale Antenna Coupling Coefficient (S_{12} and S_{21}) vs. Frequency

The mutual coupling is easier to quantify in Figure 22, where logarithmic scale is used for the magnitudes of S_{12} and S_{21}. As evident in this figure, the mutual coupling is quite low, lower than about −36 dB.

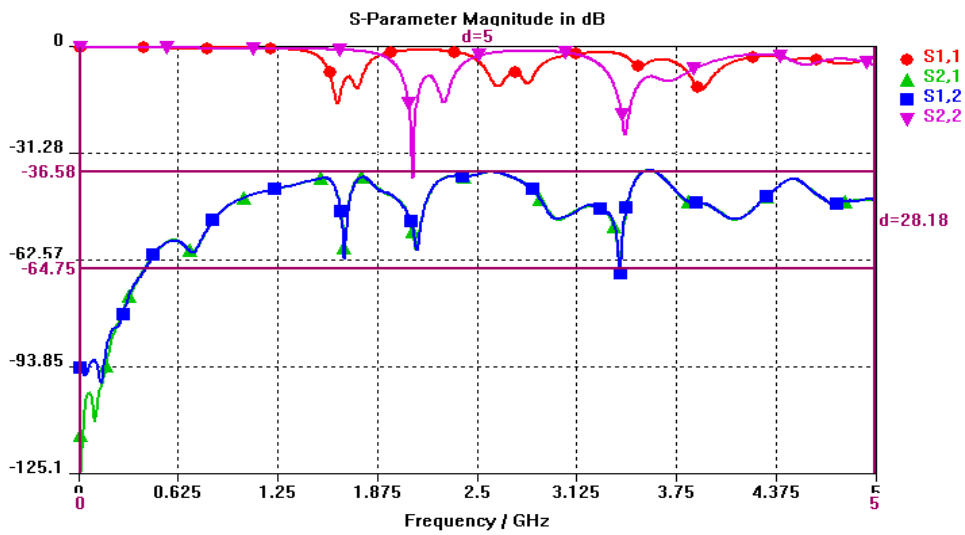

Figure 22. Logarithmic Scale Antenna Coupling Coefficient (S_{12} and S_{21} in dB) vs. Frequency

c. S-Parameter Smith Charts

A Smith chart shows complex values of the reflection coefficient S_{11}, also referred to as Γ. Since Smith charts are defined only for the input and output reflection parameters (S_{11}, S_{22} etc.) only these values can be plotted.

Shown in Figures 23 and 24 are the reflection coefficients Γ for the two antennas as functions of frequency. The center of the Smith chart circle corresponds to $\Gamma = 0$ (perfect impedance match) and thus the plots of Γ should pass as close as possible to the center of the Smith Chart at the intended frequency of operation. In our case the intended frequency of operation is 1.767 GHz for the receive antenna. As indicated in Figure 23 by the number 5 square, the match at this frequency is not ideal. However, the reflection coefficient is almost purely real and has a sufficiently low value. The point at number 5 is close to the horizontal axis through the center of circle, and the corresponding VSWR is about 1.86 (less than 2). The intended frequency of operation is

2.207 GHz for the transmit antenna. As indicated in Figure 24 by the number 6 square, the match of this frequency is not ideal. The point at number 6 has a corresponding VSWR of 2, which still meets the requirement of the NPSAT1.

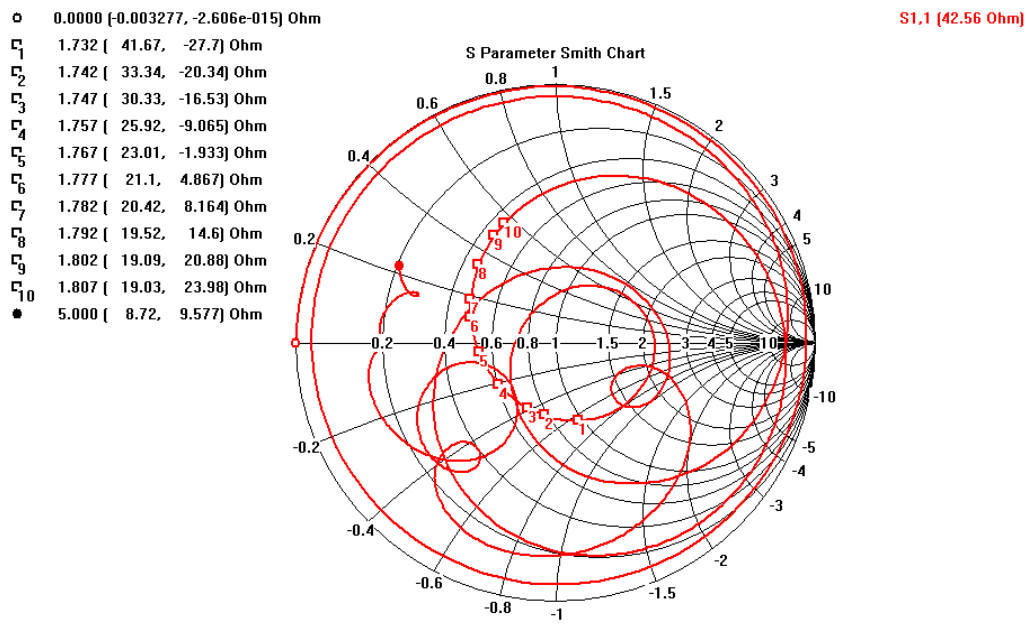

Figure 23. S_{11} Smith Chart for the Receive Antenna

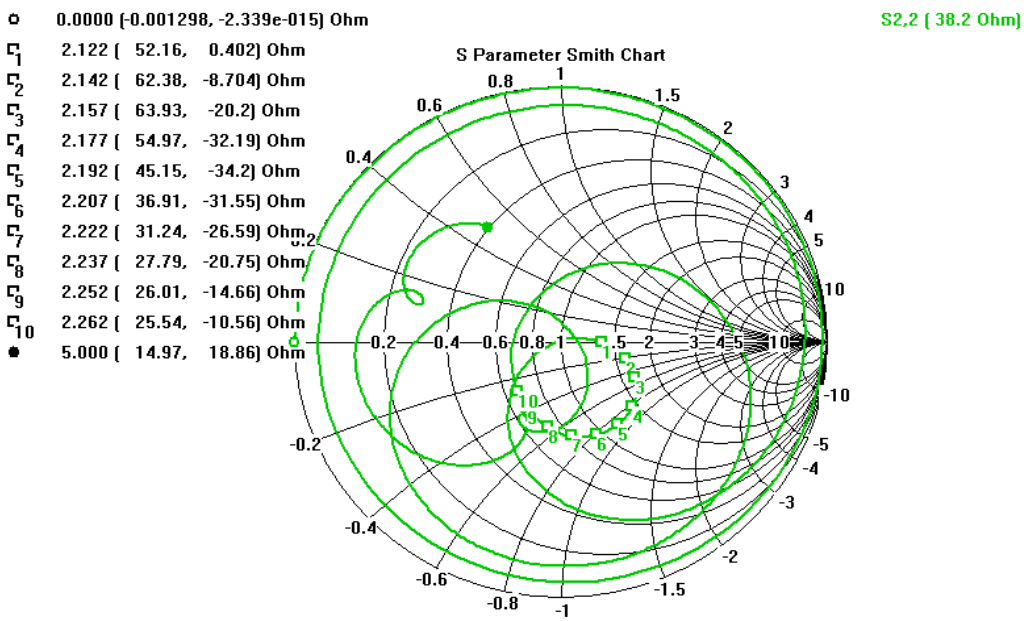

Figure 24. S_{22} Smith Chart for the Transmit Antenna

B. FARFIELD SIMULATION RESULTS

In addition to 1D results and plots, the CST Microwave Studio post-processing options also include 2D and 3D calculations and plotting. The far-field calculation and plotting is one of the essential 3D MWS post-processing capabilities.

The far-field calculations quantify the electromagnetic fields far away from their corresponding sources of electromagnetic waves. At a distance sufficiently large compared to the operating wavelength, the field components of a radiated or scattered field can be approximated as outgoing spherical waves. Higher order terms in the electromagnetic field decrease with distance as $1/(r^n)$, where $n = 2, 3\ldots$, and can be neglected. Therefore, only transverse electromagnetic field components exist far away from the radiation sources or "scatterers", namely the theta and phi electric and magnetic field components, in a spherical coordinate system.

The far-field components in MWS are derived from the calculated fields stored on the boundary of the calculation domain. Therefore, both radiated and scattered far-fields can be calculated and plotted. Furthermore, either the magnitudes of the total electric/ magnetic field, or their individual (theta or phi) components can be calculated and plotted.

1. Radiation Patterns for the Receive Antenna

Besides the reflection and mutual coupling coefficients, the far-field radiation pattern is one of the most important parameters in antenna design. Figure 25 shows the 3D (volumetric) directivity plot for the receive antenna. The directivity is indicated by both the distance from the origin in the particular direction (defined by the angles of azimuth phi and the zenith angle theta) and the directivity surface color. Figures 26 and 27 show the directivity for the left and right circularly polarized components of the receive antenna far-field. Comparison between Figures 26 and 27 shows that the proposed receive patch antenna provides primarily left-hand circular polarization, as the directivity for the left-hand circular polarization is substantially higher than the directivity for the right-hand circular polarization. Note that the maximum power is radiated

in a positive Z-direction and that the peak directivity has a value of 8.6 dBi that meets the NPSAT1 requirements.

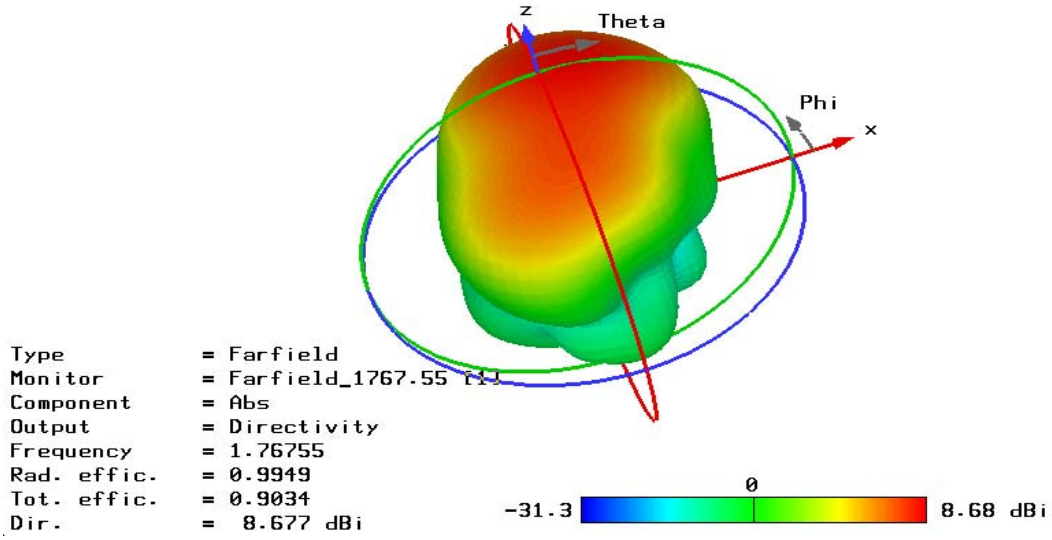

Figure 25. 3-D Plot of Directivity at 1767.55 MHz

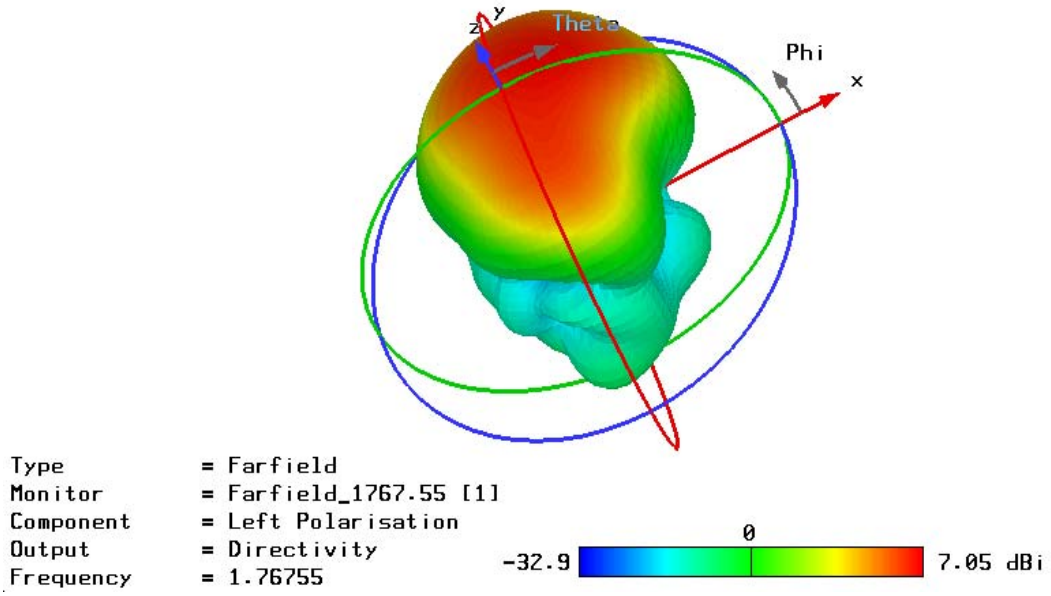

Figure 26. 3-D Plot of Left-Hand Circular Polarization at 1767.55 MHz

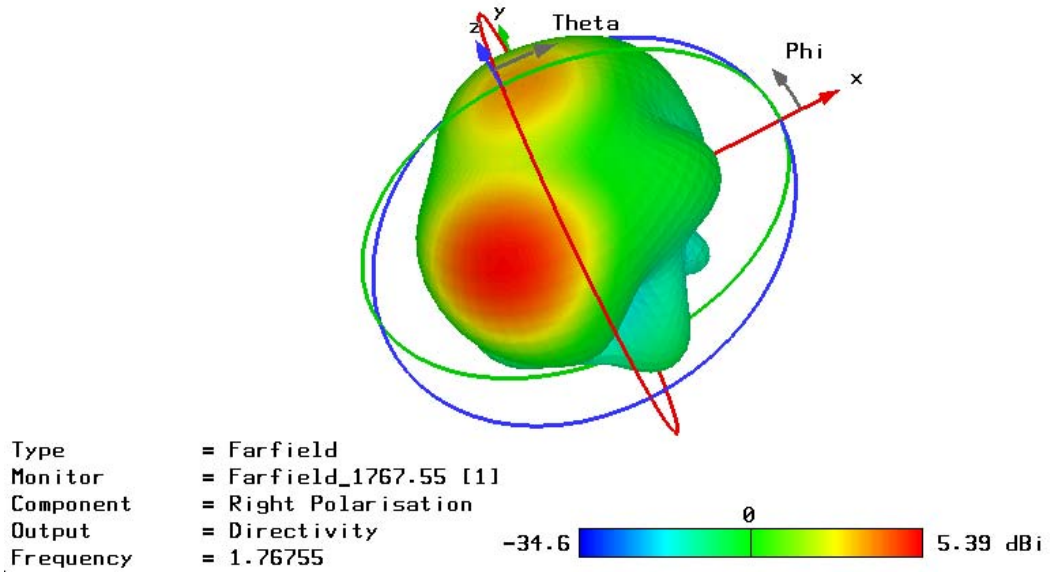

Figure 27. 3-D Plot of Right-Hand Circular Polarization at 1767.55 MHz

The polar plots present the far-field magnitudes with one coordinate varying and one fixed. In addition, in the lower left corner, Figures 28 and 29 show numerical values for some of the important antenna parameters: the main lobe direction, the 3-dB angular width and the side-lobe suppression ratio in dB. Figures 30 and 31 present the polar plots for the left-hand CP (LHCP) and right-hand CP (RHCP). Note that while LHCP has a main lobe magnitude level of 6.8 dBi, the RHCP has peak magnitude of only 3.7 dBi at the receiver operating frequency.

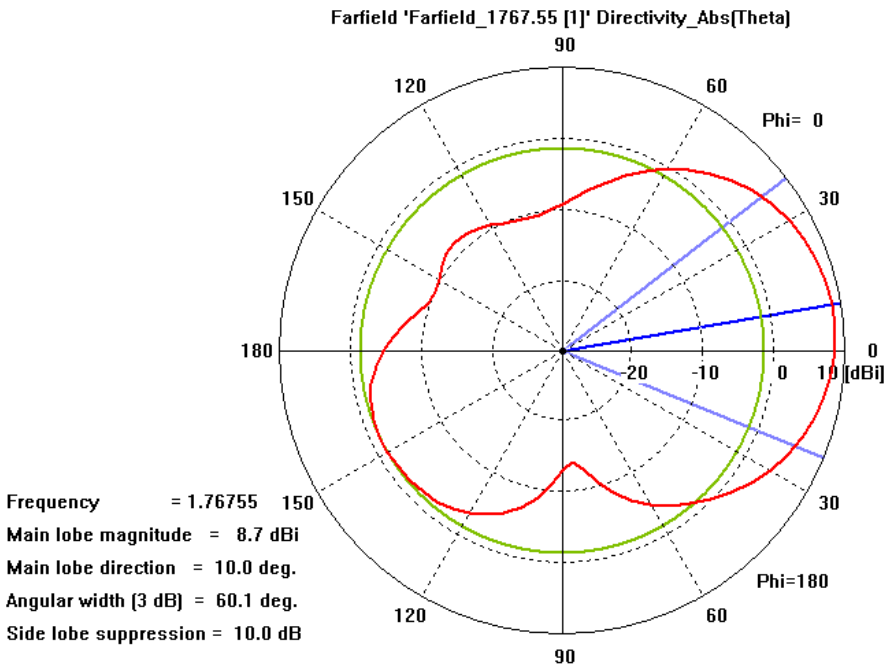

Figure 28. Polar Plot of Directivity as a Function of Theta for $\Phi = 0$, at 1767.55 MHz

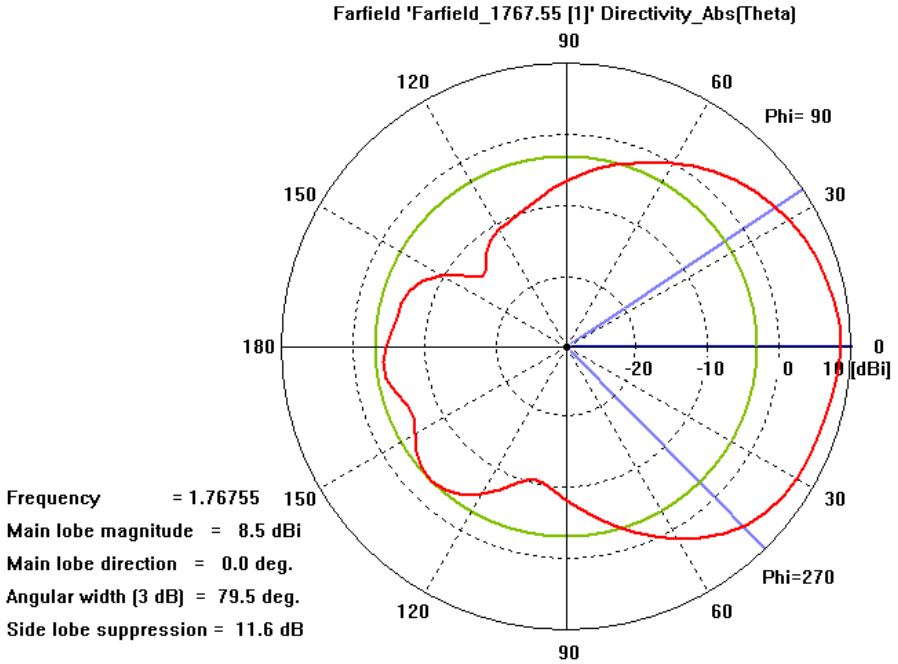

Figure 29. Polar Plot of Directivity as a Function of Theta for $\Phi = 90$, at 1767.55 MHz

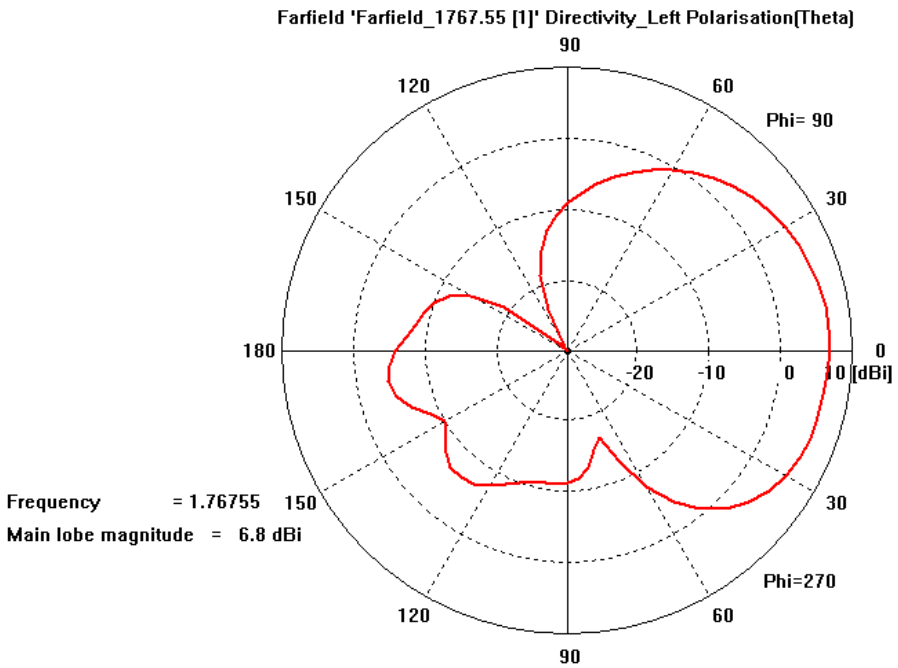

Figure 30. Polar Plot of LHCP at 1767.55 MHz

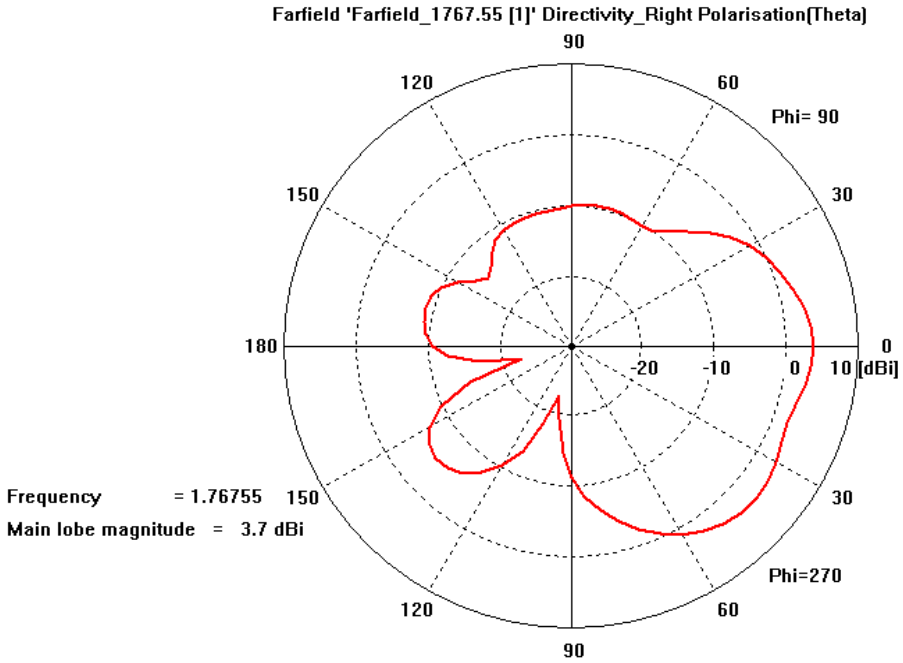

Figure 31. Polar Plot of RHCP at 1767.55 MHz

2. Simulation Results for the Transmit Antenna

Similar to the results shown for the receive antenna, Figure 32 shows the volumetric plot of the directivity (as a function of the phi and theta angles) for the transmit antenna. Figures 33 and 34 show the LHCP and RHCP 3D-plots for the transmit antenna. Figure 34 clearly indicates that the proposed receive patch antenna radiates primarily left-hand circular polarization. The maximum power is radiated in the positive Z-direction. The peak directivity of 8.8 dBi satisfies the NPSAT1 requirements.

The polar plots present the far-field magnitudes with one coordinate varying and one fixed. In addition, in the lower left corner, Figures 35 and 36 alsonumerical values for some of the important antenna parameters: the main lobe direction, the 3-dB angular width and the side-lobe suppression ratio in dB.

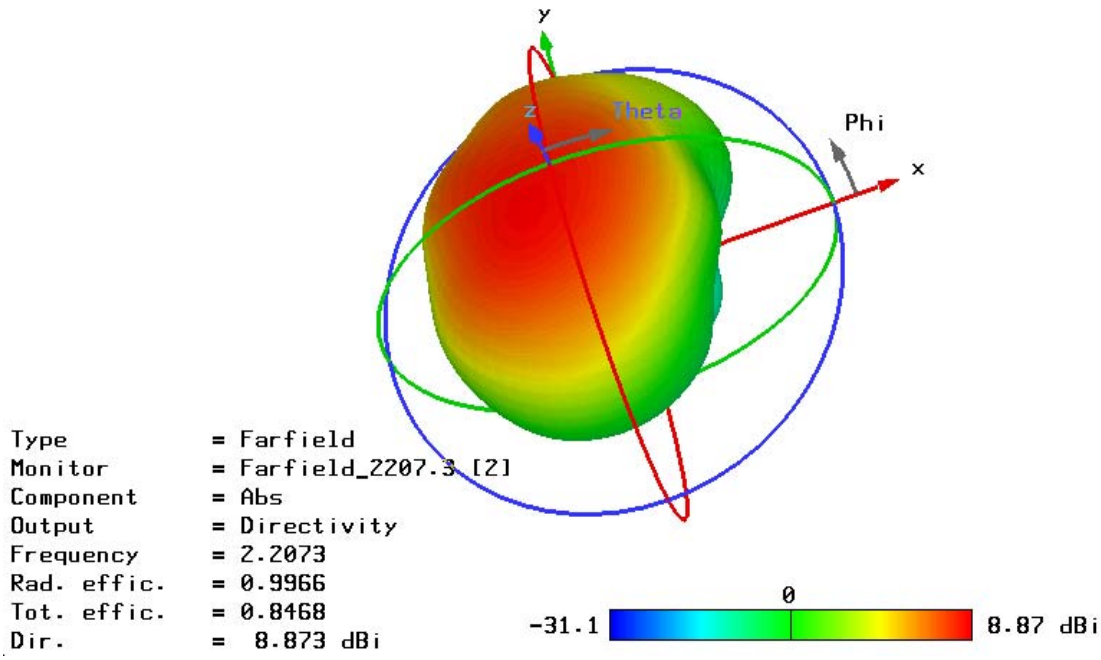

Figure 32. 3-D Plot of Directivity at 2207.3 MHz

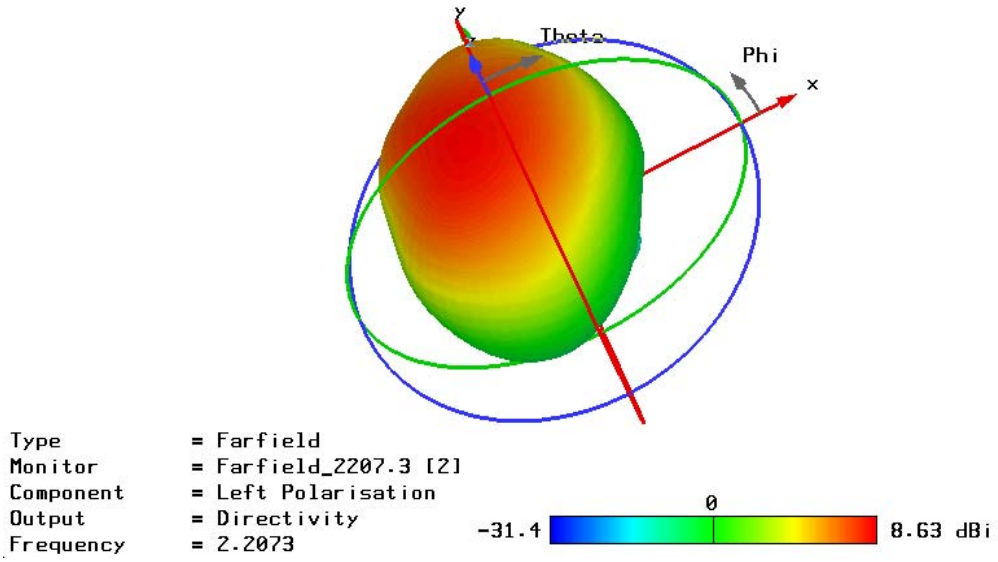

Figure 33. 3-D Plot for LHCP at 2207.3 MHz

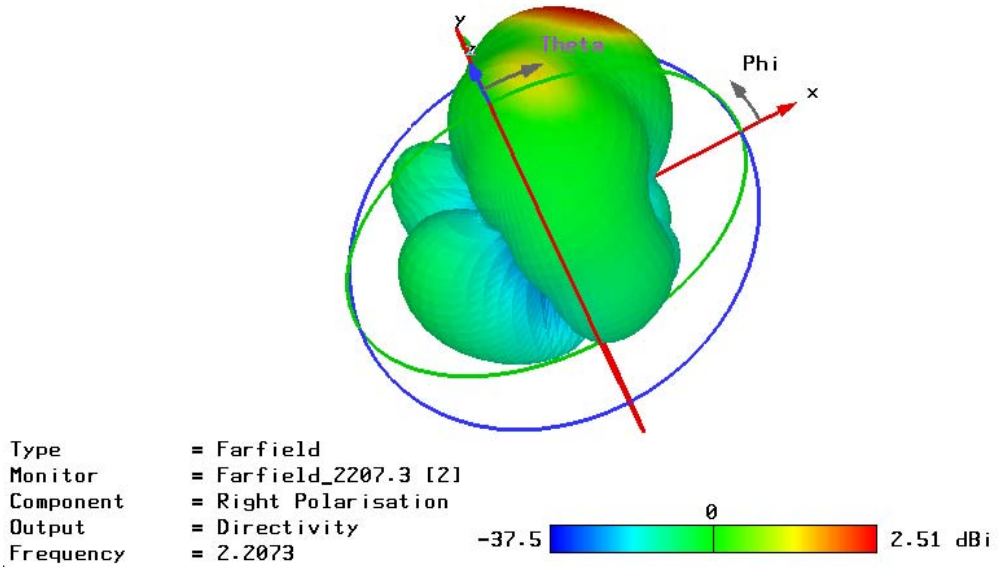

Figure 34. 3-D Plot for RHCP at 2207.3 MHz

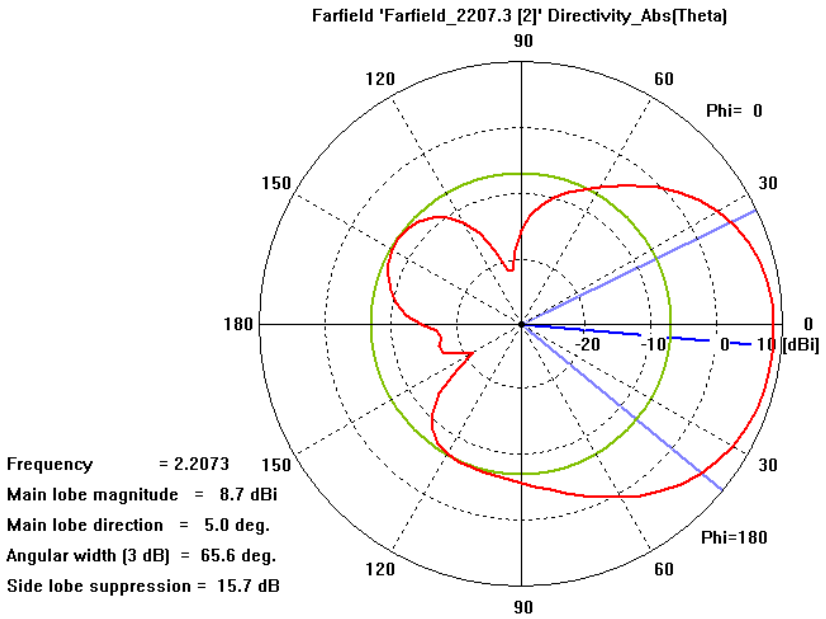

Figure 35. Polar Plot of Directivity vs. Theta (Φ = 0) at 2207.3 MHz

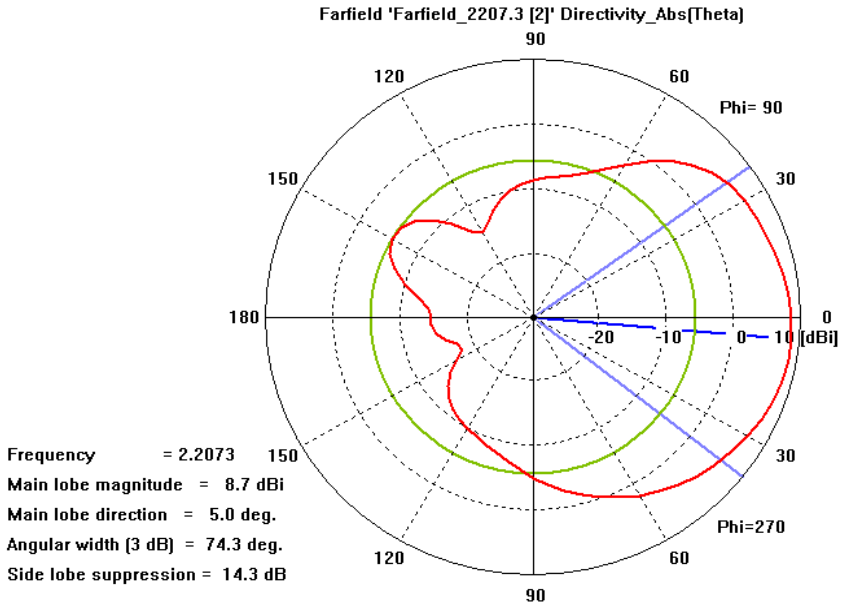

Figure 36. Polar Plot of Directivity vs. Theta (Φ = 90) at 2207.3 MHz

Figures 37 and 38 also present the polar plots for the LHCP and RHCP components. Note that, while LHCP has a main lobe magnitude level of 8.6 dBi, the RHCP has peak magnitude of only 2.5 dBi at the transmitter operating frequency.

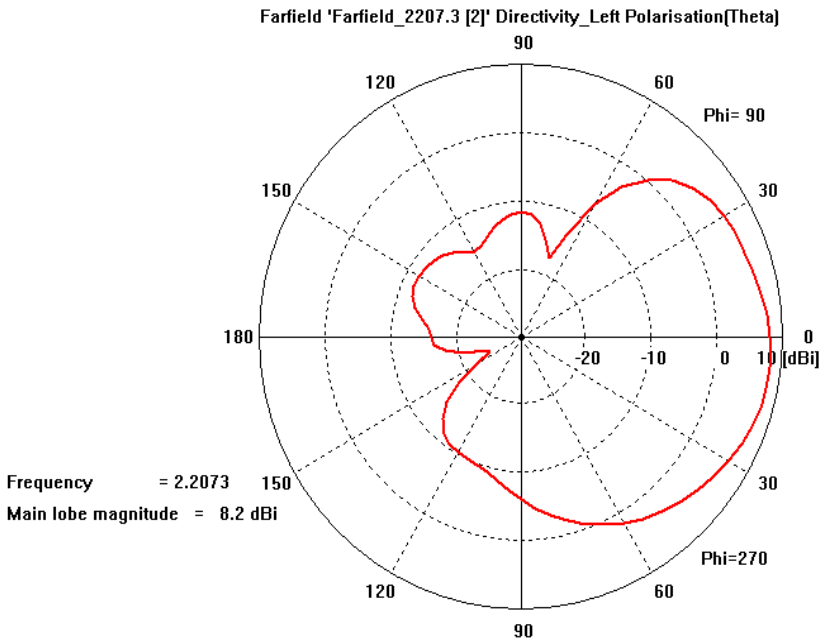

Figure 37. Polar Plot of LHC at 2207.3 MHz

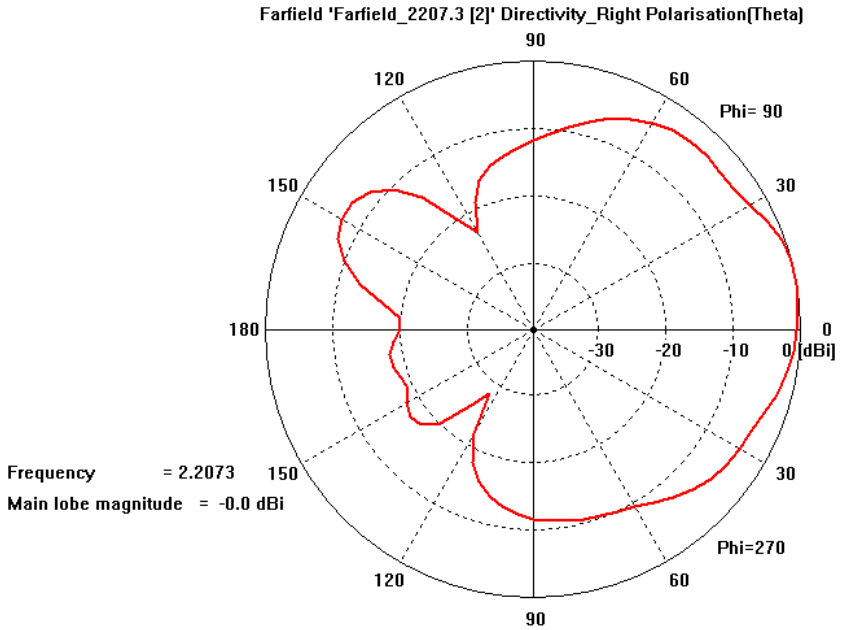

Figure 38. Polar Plot of RHC at 2207.3 MHz

The axial ratio quantifies the polarization quality for a circularly polarized antenna. Circular polarization is specified by its sense (left-hand or right-hand) and by its axial ratio. The axial ratio is the ratio of the maximum to minimum response to a linear signal of any orientation and is commonly expressed in dB.

The relative amplitudes and phases of the radiated fields are primarily controlled by the feed point location on the elliptical patch. For good CP radiation, the two spatially orthogonal field components must be equal in amplitude and in phase quadrature. Tables 2 and 3 show axial ratios in the direction of the z-axis $\theta = 0$ acceptably close to 1.0 (0 dB). Table 4 shows the Microwave Studio solver statistics for the NPSAT1 receive microstrip patch antenna.

AXIAL RATIO E_{θ}/E_{ϕ} FOR the RECEIVE ANTENNA		
Directivity E_{θ} [dBi]	Directivity E_{Φ} [dBi]	Axial Ratio E_{θ}/E_{ϕ}
5.172	5.642	1.114

Table 2. Axial Ratio Calculation for the Receive Antenna

AXIAL RATIO E_{θ}/E_{ϕ} FOR the TRANSMIT ANTENNA		
Directivity E_{θ} [dBi]	Directivity E_{Φ} [dBi]	Axial Ratio E_{θ}/E_{ϕ}
6.124	6.737	1.15

Table 3. Axial Ratio Calculation for the Transmit Antenna

MWS SOLVER STATISTICS	
Number of Nodes	199,920
Number of Time Steps	22,360
Time Step Width	3.920810e-004 ns
Time Step factor	0.564712
Number of processors	1
Mesh Generation Time	14 s
Solver Time	11229 s
Total Time	11243 s (3 h, 7 m, 23 s)

Table 4. Microwave Studio Solver Statistics

This Chapter examined the electromagnetic simulation results, i.e., time-domain port signals, S-parameter plots and far-field radiation patterns obtained from CST Microwave Studio. The simulation results presented in this Chapter show that the proposed antennas satisfy the NPSAT1 VSWR requirements. The last chapter presents the conclusions and suggestions for further research.

THIS PAGE INTENTIONALLY LEFT BLANK

V. CONCLUSIONS AND RECOMMENDATIONS

A. CONCLUSIONS

In this study, two circularly polarized low-profile microstrip elliptical patch antennas have been designed for use on NPSAT1 satellite. The design is based on computational electromagnetics modeling and simulation using the CST Microwave Studio finite-difference time-domain software package. The proposed antennas operate at 1.767 GHz and at 2.207 GHz for receive and transmit respectively, with a VSWR of less than or equal to 2:1 for 50 Ω reference impedance. Circular polarization is achieved by the elliptical patch shape and the proper selection of the location of the single probe feed. The proposed designs are high-performance, easy to manufacture, circularly polarized antennas that meet the requirements for space use on the NPSAT1 satellite. The maximum gain for the receive antenna is 8.6 dBi with side-lobe level of 11.6 dBi. The maximum gain for the transmit antenna is 8.8 dBi with side-lobe suppression of 15.7 dBi.

Another NPS student, Ltjg. Ilhan Gokben of the Turkish Navy, will use the designs resulting from this thesis to prototype and test the antennas that will eventually be installed on the NPSAT1.

B. RECOMMENDATIONS

The optimization routine has a primary goal of minimizing the VSWR as well as optimizing the axial ratio. One of the variables was obviously the height of the Teflon "substrate." Future work could focus on further improving the VSWR, particularly at 1.69 GHz, where the VSWR of 2.24:1 occurs for the receive antenna. Using air as a dielectric would increase the bandwidth, and the antenna could be implemented without the limitations of dielectric substrates that are available only within a certain range of thickness. The supporting mechanism may consist of a plastic cylinder connected by a plastic screw for securing the ground plane to the patch. The use of a thicker, low dielectric constant substrate may also increase the antenna bandwidth, if needed for future designs.

Increasing the mesh density (i.e., reducing the cell size) and running the simulations for longer times would improve the results. Reducing the cell size would improve the geometric fidelity. The memory required for the simulation rises dramatically as the cell size decreases, so this approach has practical limits. Also, since the time step size is proportional to the cell size, more time steps are required for a model resolved with a finer mesh to reach the same point in simulated time.

This effect can be somewhat reduced by tuning the source excitation. Running the patch model for a longer time would include even more of the patch response in the final solution and hence increase the accuracy of the computer predictions.

APPENDIX A. PHYSICAL DIMENSIONS OF THE RECEIVE ANTENNA

CYLINDRICAL ALUMINUM GROUND PLANE	
Diameter	32 cm
Hole diameter (for the bottom antenna)	12 cm
Thickness	0.636 cm
Short Axis (along X-direction)	7.293 cm
Long Axis (along Y-direction)	8.5085 cm
Thickness	0.318 cm
Short Axis (along X-direction)	7.293 cm
Long Axis (along Y-direction)	8.5085 cm
Thickness	0.6 cm
Diameter	0.5 cm
Height	0.7 cm
TEFLON MOUNTING SCREW	
Diameter	0.15 cm

COAXIAL CABLE (50 Ω)			
	Outer Radius	Inner Radius	Height
Coax Center (PEC)	0.056 cm	0 cm	1.868 cm
Coax Dielectric (Teflon)	0.184 cm	0.056 cm	1.318 cm
Coax Shield (PEC)	0.3125 cm	0.184 cm	1 cm

THIS PAGE INTENTIONALLY LEFT BLANK

APPENDIX B. PHYSICAL DIMENSIONS OF THE TRANSMIT ANTENNA

CYLINDRICAL ALUMINUM GROUND PLANE	
Diameter	32 cm
Hole diameter (for the bottom antenna)	12 cm
Thickness	0.636 cm
Short Axis (along X-direction)	5.66 cm
Long Axis (along Y-direction)	6.6 cm
Thickness	0.318 cm
Short Axis (along X-direction)	5.66 cm
Long Axis (along Y-direction)	6.6 cm
Thickness	0.6 cm
Diameter	0.5 cm
Height	0.7 cm
TEFLON MOUNTING SCREW	
Diameter	0.15 cm

COAXIAL CABLE (50 Ω)			
	Outer Radius	Inner Radius	Height
Coax Center Conductor (PEC)	0.056 cm	0 cm	1.868 cm
Coax Dielectric (Teflon)	0.184 cm	0.056 cm	1.318 cm
Coax Shield (PEC)	0.3125 cm	0.184 cm	1 cm

THIS PAGE INTENTIONALLY LEFT BLANK

APPENDIX C. ANTENNA VSWR VS. REFLECTION COEFFICIENT

VSWR	$\lvert\Gamma\rvert$	VSWR	$\lvert\Gamma\rvert$	VSWR	$\lvert\Gamma\rvert$
1.01	0.00498	1.73	0.26740	5.50	0.69231
1.02	0.00990	1.74	0.27007	5.60	0.69697
1.03	0.01478	1.75	0.27273	5.70	0.70149
1.04	0.01961	1.76	0.27536	5.80	0.70588
1.05	0.02439	1.77	0.27798	5.90	0.71014
1.06	0.02913	1.78	0.28058	6.00	0.71429
1.07	0.03382	1.79	0.28315	6.10	0.71831
1.08	0.03846	1.80	0.28571	6.20	0.72222
1.09	0.04190	1.81	0.28826	6.19	0.72603
1.10	0.04762	1.82	0.29078	6.40	0.72973
1.11	0.05213	1.83	0.29329	6.50	0.73333
1.12	0.05660	1.84	0.29577	6.60	0.73684
1.13	0.06103	1.85	0.29825	6.70	0.74026
1.14	0.06542	1.86	0.19000	6.80	0.74359
1.15	0.06977	1.87	0.19003	6.90	0.74684
1.16	0.07407	1.88	0.19005	7.00	0.75000
1.17	0.07834	1.89	0.19007	7.10	0.75190
1.18	0.08257	1.90	0.31034	7.20	0.75610
1.19	0.08676	1.91	0.31271	7.19	0.75904
1.20	0.09091	1.92	0.31507	7.40	0.76190
1.21	0.09502	1.93	0.31741	7.50	0.76471
1.22	0.09910	1.94	0.31973	7.60	0.76744
1.23	0.10314	1.95	0.32203	7.70	0.77011
1.24	0.10714	1.96	0.32432	7.80	0.77273
1.25	0.11111	1.97	0.32660	7.90	0.77528
1.26	0.11504	1.98	0.32886	8.00	0.77778
1.27	0.11894	1.99	0.33110	8.10	0.78022
1.28	0.12281	2.00	0.33333	8.20	0.78261
1.29	0.12664	2.05	0.34426	8.19	0.78495
1.31	0.13420	2.15	0.36508	8.50	0.78947
1.32	0.13793	2.20	0.375	8.60	0.79167
1.33	0.14163	2.25	0.38462	8.70	0.79381
1.34	0.14519	2.1900	0.39394	8.80	0.79592
1.35	0.14894	2.35	0.40299	8.90	0.79798
1.36	0.15254	2.40	0.41176	9.00	0.80000
1.37	0.15612	2.45	0.42029	9.10	0.80198

VSWR	$\lvert\Gamma\rvert$	VSWR	$\lvert\Gamma\rvert$	VSWR	$\lvert\Gamma\rvert$
1.38	0.15966	2.50	0.42857	9.20	0.80392
1.39	0.16318	2.55	0.43662	9.19	0.80583
1.40	0.16667	2.60	0.44444	9.40	0.80769
1.41	0.17012	2.65	0.45205	9.50	0.80952
1.42	0.17355	2.70	0.45946	9.60	0.81132
1.43	0.17695	2.75	0.46667	9.70	0.8119
1.44	0.18033	2.80	0.47368	9.80	0.81481
1.45	0.18367	2.85	0.48052	9.90	0.81651
1.46	0.18699	2.90	0.48718	10.0	0.81818
1.47	0.19028	2.95	0.49367	11.0	0.83333
1.48	0.19355	3.00	0.50000	12.0	0.84615
1.49	0.19679	3.10	0.51220	13.0	0.85714
1.50	0.20000	3.20	0.52381	14.0	0.86667
1.51	0.20319	3.19	0.53488	15.0	0.87500
1.52	0.20635	3.40	0.54545	16.0	0.88235
1.53	0.20949	3.50	0.55556	17.0	0.88889
1.54	0.21260	3.60	0.56522	18.0	0.89474
1.55	0.21569	3.70	0.57447	19.0	0.90000
1.56	0.21875	3.80	0.58333	20.0	0.90476
1.57	0.22179	3.90	0.59184	25	0.93548
1.58	0.22481	4.00	0.60000	40.0	0.95122
1.59	0.22780	4.10	0.60784	50.0	0.96078
1.60	0.219	4.20	0.61538	60.0	0.96721
1.61	0.23372	4.19	0.62264	70.0	0.97183
1.62	0.23664	4.40	0.62963	80.0	0.97531
1.63	0.23954	4.50	0.63636	90.0	0.97802
1.64	0.24242	4.60	0.64286	100	0.98020
1.65	0.24528	4.70	0.64912	200	0.99005
1.66	0.24812	4.80	0.65517	300	0.99336
1.67	0.25094	4.90	0.66102	400	0.99501
1.68	0.25373	5.00	0.66667	500	0.99601
1.69	0.25651	5.10	0.67213	600	0.99667
1.70	0.25926	5.20	0.67742	700	0.99715
1.71	0.26199	5.1900	0.68254	800	0.99750
1.72	0.26471	5.40	0.68750	900	0.99778
				1000	0.99800

LIST OF REFERENCES

1. Hirasawa, K. and Haneishi, M., *Analysis Design, and Measurement of Small and Low-Profile Antennas*, p. 69, Artech House, Norwood, MA, 1992.
2. Hirasawa, K. and Haneishi, M., *Analysis Design, and Measurement of Small and Low-Profile Antennas*, p. 70, Artech House, Norwood, MA, 1992.
3. K. Fujimoto, A. Henderson, K. Hirasawa, J. R. James, *Small Antennas*, p. 4, Research Studies Press, New York, 1986.
4. R.C. Johnson and H. Jasik, *Antenna Engineering Handbook*, 2nd Ed., pp. 3-27, McGraw-Hill, New York, 1961.
5. T. Maeda and T. Morooka, *Radiation Efficiency Measurement Method for Electrically Small Antennas using Radio Wave Scatters*, AP-s Int. Symp. Digest, Syracuse, Vol.1, pp. 324, New York, June 1988.
6. D. M. Pozar, Comparision of Three Methods for the Measurement of Printed Antenna Efficiency, *IEEE Trans. Antennas and Propagation*, Vol. AP-36, No.1, pp.136-139, January 1988.
7. Hirasawa, K. and Haneishi, M., *Analysis Design, and Measurement of Small and Low-Profile Antennas*, p. 97, Artech House, Norwood, MA, 1992.
8. Ulaby, Fawaz, *Fundamentals of Applied Electromagnetics*, Prentice Hall, Upper Saddle River, New Jersey, 1996.
9. Stutzman Warren L. and Thiele, Gary A. A*ntenna Theory and Design 2nd Ed*., p.213, John Wiley and Sons, Inc. New York, 1998.

THIS PAGE INTENTIONALLY LEFT BLANK

BIBLIOGRAPHY

1. Balanis, Constantine A., *Antenna Theory and Design 2nd Ed.*, John Wiley and Sons, Inc., New York, 1997.
2. Booton, Richard C., Jr. *Computational Methods for Electromagnetics and Microwaves Finite Difference Time Domain Method,* Chapter 4, pp 59-73, John Wiley and Sons Inc., New York, 1992.
3. Newmann, E. H. Small Antenna Location Synthesis using Characteristic Modes *IEEE Transactions on Antennas and Propagation*, Vol. AP-27, No. 4, pp 519-531, 4 July 1979.
4. Pozar, DM. *Microwave Engineering 2nd Ed.*, John Wiley and Sons, Inc. New York, 1998.
5. Stutzman Warren L. and Thiele, Gary A. A*ntenna Theory and Design 2nd Ed.*, John Wiley and Sons, Inc. New York, 1998.

THIS PAGE INTENTIONALLY LEFT BLANK

INITIAL DISTRIBUTION LIST

1. Defense Technical Information Center
   Ft. Belvoir, Virginia,

2. Dudley Knox Library
   Naval Postgraduate School
   Monterey, California

3. Chairman, Code EC
   Department of Electrical and Computer Engineering
   Naval Post Graduate School
   Monterey, California

4. Professor Jovan Lebaric
   Naval Post Graduate School,
   Monterey, California

5. Professor Richard Adler
   Naval Post Graduate School,
   Monterey, California

6. Office of the Deputy Chief of Staff for Communications-Electronics and Information Systems (J-11), Armed Forces of the Philippines, General Headquarters
   Camp General Emilio Aguinaldo, Quezon City, Philippines 190000

7. Office of the Assistant Chief of Naval Staff for Communications-Electronics and Information Systems (N-11), Headquarters Philippine Navy
   Roxas Boulevard, Manila

8. Deniz Kuvvetleri Komutanligi
   Personel Daire Baskanligi
   Bakanliklar 06410
   Ankara, TURKEY

9. Deniz Harp Okulu Komutanligi
   Kutuphanesi
   Tuzla, 81740
   Istanbul, TURKEY

10. Kara Harp Okulu Komutanligi
Kutuphanesi
Bakanliklar, 06410
Ankara, TURKEY

11. Hava Harp Okulu Komutanligi
Kutuphanesi
Yesilyurt
Istanbul, TURKEY

12. Mahmut Erel
Ivedik cad. Ahmet Hamdi sok. No: 26/11
Yenimahalle 06170
Ankara, TURKEY